Breakdown of Immune Tolerance in AIRE-Deficient Rats Induces a Severe Autoimmune Polyendocrinopathy–Candiasis–Ectodermal Dystrophy–like Autoimmune Disease

Jason Ossart, Anne Moreau, Elodie Autrusseau, Séverine Ménoret, Jérôme C. Martin, Marine Besnard, Laure-Hélène Ouisse, Laurent Tesson, Léa Flippe, Kai Kisand, Pärt Peterson, François-Xavier Hubert, Ignacio Anegon, Régis Josien and Carole Guillonneau

J Immunol published online 29 June 2018
http://www.jimmunol.org/content/early/2018/06/28/jimmunol.1701318

The Journal of Immunology is published twice each month by
The American Association of Immunologists, Inc.,
1451 Rockville Pike, Suite 650, Rockville, MD 20852

Print ISSN: 0022-1767 Online ISSN: 1550-6606.

Published June 29, 2018, doi:10.4049/jimmunol.1701318

Breakdown of Immune Tolerance in AIRE-Deficient Rats Induces a Severe Autoimmune Polyendocrinopathy–Candiasis–Ectodermal Dystrophy–like Autoimmune Disease

Jason Ossart,*,† Anne Moreau,‡ Elodie Autrusseau,*,† Séverine Ménoret,*,†,§ Jérôme C. Martin,*,† Marine Besnard,*,† Laure-Hélène Ouisse,*,†,§ Laurent Tesson,*,†,§ Léa Flippe,*,† Kai Kisand,¶ Pärt Peterson,¶ François-Xavier Hubert,*,† Ignacio Anegon,*,†,§ Régis Josien,*,†,‖ and Carole Guillonneau*,†

Autoimmune regulator (AIRE) deficiency in humans induces a life-threatening generalized autoimmune disease called autoimmune polyendocrinopathy–candidiasis–ectodermal dystrophy (APECED), and no curative treatments are available. Several models of AIRE-deficient mice have been generated, and although they have been useful in understanding the role of AIRE in central tolerance, they do not reproduce accurately the APECED symptoms, and thus there is still a need for an animal model displaying APECED-like disease. We assessed, in this study, the potential of the rat as an accurate model for APECED. In this study, we demonstrate that in rat, AIRE is expressed by MHC class II (MCH-II)$^+$ and MHC-II$^-$ medullary thymic epithelial cells in thymus and by CD4^{int} conventional dendritic cells in periphery. To our knowledge, we generated the first AIRE-deficient rat model using zinc-finger nucleases and demonstrated that they display several of the key symptoms of APECED disease, including alopecia, skin depigmentation, and nail dystrophy, independently of the genetic background. We observed severe autoimmune lesions in a large spectrum of organs, in particular in the pancreas, and identified several autoantibodies in organs and cytokines such as type I IFNs and IL-17 at levels similar to APECED. Finally, we demonstrated a biased Ab response to IgG1, IgM, and IgA isotypes. Altogether, our data demonstrate that AIRE-deficient rat is a relevant APECED animal model, opening new opportunity to test curative therapeutic treatments. *The Journal of Immunology*, **2018, 201: 000–000.**

Breakdown of self-tolerance leads to a dysfunction of the immune system and is the cause of development of autoimmune diseases that have serious, disabling, and even fatal consequences. In contrast, an increase of the mechanisms of immune tolerance to nonself would also be beneficial in the context of organ and bone marrow transplantation, allergy, and gene therapy. Thus, a better knowledge of immunological mechanisms involved in tolerance represents a major challenge to improve both the understanding and treatment of autoimmune diseases. A key player in this equilibrium is the autoimmune regulator (AIRE), a transcription regulator that allows the expression of tissue-restricted Ags in medullary thymic epithelial cells (mTECs) (1, 2) and autoreactive T cell deletion. The autoimmune polyendocrinopathy-candidiasis-ectodermal dystrophy (APECED) syndrome, also known as autoimmune polyglandular syndrome type I, is a rare multiorgan autosomal recessive autoimmune disease caused by mutations in the *Aire* gene (3). In humans, this gene is located on locus 21q22.3 (4, 5) and more than 100 mutations have been described to cause APECED, with a prevalence of 1–9:1,000,000 (Orphanet, http://www.orpha.net); however, it is increased in certain populations, such as the Finnish, Norwegian, Sardinian, and Iranian Jewish populations, because of consanguinity or founder effects (6–8). Among Sardinians,

*Centre de Recherche en Transplantation et Immunologie UMR 1064, INSERM Université de Nantes, 44093 Nantes, France; †Institut de Transplantation Urologie Néphrologie, CHU Nantes, 44093 Nantes, France; ‡Anatomie et Cytologie Pathologiques, CHU Nantes, 44093 Nantes, France; §Transgenesis Rat Immunophenomic Platform, INSERM 1064 and SFR Francois Bonamy, CNRS UMS3556, 44093 Nantes, France; ¶Molecular Pathology, Institute of Biomedicine and Translational Medicine, University of Tartu, Tartu 50411, Estonia; and ‖Laboratoire d'Immunologie, CHU Nantes, 44093 Nantes, France

ORCIDs: 0000-0002-9200-4927 (S.M.); 0000-0003-0068-8776 (J.C.M.); 0000-0002-4058-2848 (L.-H.O.); 0000-0002-5426-4648 (K.K.); 0000-0001-6755-791X (P.P.); 0000-0001-7900-7413 (R.J.).

Received for publication September 15, 2017. Accepted for publication June 2, 2018.

This work was supported by the National Research Agency, in the context of the Laboratoire d'Excellence Immunotherapy Graft Oncology program, via the investment of future program Contract ANR-11-LABX-0016-01 and under the auspices of the Institut Hospitalo-Universitaire–Centre Européen des Sciences de Transplantation et Immunothérapie (IHU-CESTI) project, which received French government financial support managed by the National Research Agency (ANR) via the investment of future program Contract ANR-10-IBHU-005. The IHU-CESTI project is also supported by Nantes Metropole and the Pays de la Loire Region. This work was also performed in the context of the Transgenèse pour les Etudes Fonctionnelles sur les Organismes Modèles project funded by the Investissements d'Avenir French Government program, managed by the ANR (Contract ANRII-INSB-0014). The study was also supported by Estonian Research Agency (Contract IUT2-2). For this work, J.O. was supported by Fondation pour la Recherche Médicale Contract PLP20141031245, and F.-X.H. was supported by a Marie Curie Outgoing Fellowship from the Framework Program 6. The Fondation Progreffe also provided financial support.

The sequences presented in this article have been submitted to the European Nucleotides Archive (https://www.ebi.ac.uk/ena) under accession number ERP107351.

Address correspondence and reprint requests to Dr. Carole Guillonneau, Centre de Recherche en Transplantation et Immunologie UMR 1064, ITUN, 30 Boulevard Jean Monnet, 44093 Nantes Cedex 01, France. E-mail address: carole.guillonneau@univ-nantes.fr

The online version of this article contains supplemental material.

Abbreviations used in this article: AIRE, autoimmune regulator; ALN, axillary lymph node; APECED, autoimmune polyendocrinopathy–candidiasis–ectodermal dystrophy; BN, Brown Norway; cDC, conventional dendritic cell; DC, dendritic cell; DGE, digital gene expression; HES, hematoxylin eosin saffron; KLH, keyhole limpet hemocyanin; LIPS, luciferase immunoprecipitation system; MHC-II, MHC class II; MLN, mesenteric lymph node; mTEC, medullary thymic epithelial cell; NLS, nuclear localization signal; SPD, Sprague Dawley; Treg, regulatory T cell; WT, wild type; ZFN, zinc-finger nuclease.

the overrepresentation of the R139X mutation is observed present, for instance, in 90% of Sardinian APECED patients (8). The clinical phenotype of APECED is usually defined by the presence of two of the three major symptoms: hypoparathyroidism, adrenal insufficiency (Addison disease), and chronic mucocutaneous candidiasis (7). This disease is also associated with anti-cytokine Abs (present in all patients and particularly directed to IFN-α and -ω) and multiple autoimmune and ectodermal features such as type 1 diabetes, enamel hypoplasia, vitiligo, premature ovarian failure, keratitis, pernicious anemia, alopecia, exocrine pancreatitis, interstitial lung disease, nephritis, and others (7, 9–13).

Because of the identification of the link between APECED and AIRE (4, 14), several mouse models of AIRE deficiency have been developed (15). These models have been important in the characterization of the role of AIRE in thymic-negative selection of T lymphocytes and regulatory T cell (Treg) differentiation. The first *Aire*$^{-/-}$ mice showed a slight lymphocyte infiltration in the liver of some animals, and a few animals displayed circulating autoantibodies (16). Other AIRE-deficient mice displayed more features of APECED, especially the NOD strain mice (1, 17).

In this article, to our knowledge, we described the first rat model of AIRE deficiency, which we have generated using the zinc-finger nucleases (ZFN) technology. In this study, we show, in the rat, predominant AIRE expression in the thymus by CD45^{-} cells and in the periphery by CD4^{int} conventional dendritic cells (cDCs), a pattern similar to that reported in humans. We demonstrate that two strains of *Aire*$^{-/-}$ rats developed strong autoimmune symptoms characteristic of APECED, such as alopecia and vitiligo, numerous circulating autoantibodies, leukocyte infiltrates, lesions in several organs, and impaired thymus development. We also observed a biased Ig isotype production, changes in several immune cell subsets, and an increase in cytokines. Altogether, these results demonstrate the *Aire*$^{-/-}$ rats present several features of human APECED and will improve our understanding of the disease and of the mechanisms of action of AIRE.

Materials and Methods

Rats

Aire knockout rats (Brown Norway [BN], inbred strain) were generated by a targeted disruption of the *Aire* gene using ZFNs as previously described (18). The ZFNs were purchased from Sigma-Aldrich (St. Louis, MO) and were mutated (EL:KK) obligate heterodimers, reducing potential off targets (and are predicted to bind to a DNA sequence 5′-TGCCACCCA-GACCCCCCACAAAGAGAAGAGCCCTGGAAGAG-3′ in exon 3 of the *Aire* gene. Off-target edits by the nucleases were analyzed in silico and were all contained within introns and intergenic noncoding regions in chromosomes other than chromosome 20, where the *Aire* gene is located (data not shown). These rats were backcrossed in a Sprague Dawley (SPD; outbred strain) background for six generations to obtain AIRE-deficient SPD rats. All animals were used at >6 mo of age unless indicated otherwise. All studies were performed according to protocols approved by the Ethics Committee of the Ministère de l'Enseignement Supérieur et de la Recherche (Paris, France).

Genotyping

Ear biopsy specimens from 8- to 10-d-old rats were digested in 300 μl of tissue digestion buffer (Tris-HCl 0.1 mol/l [pH 8.3], EDTA 5 mmol/l, SDS 0.2%, NaCl 0.2 mol/l, PK 100 μg/ml) in a 1.5-ml tube at 56°C overnight.

PCR amplification was performed with 1:20 dilution of the lysis product and 25 μl of PCR reaction mix according to the manufacturer instruction (Herculase II Fusion DNA Polymerase, Agilent Technologies) using the following PCR primers: forward 5′-TCAAGAGTGCCCTGTTCTAG-3′ and reverse 5′-CTGGGGTGGTGTCAGTAAG-3′. The following amplification program was used: 1 cycle at 95°C for 5 min, 35 cycles of 98°C for 10 s, 60°C for 10 s, and 72°C for 30 s, followed by 1 cycle at 72°C for 4 min using a Veriti Thermal Cycler (Applied Biosystems, Foster City, CA).

The PCR products were analyzed by heteroduplex mobility assay using microfluidic capillary electrophoresis using a microchip capillary electrophoresis system caliper LabChip GX (PerkinElmer). The microfluidic 5K was loaded with gel and marker in the specified containers according to the manufacturer's protocol. PCR tube strips or plates were centrifuged (5 min, 2000 rpm) and placed without caps or adhesive film in the electrophoresis system. Each sample was mixed automatically with an internal marker and run through these microcapillaries according to their sizes and nucleotidic compositions. The DNA fluorescence measurement was recorded as a function of time on an electrophoregram, and the DNA ladder defined the product sizes. The software then generated a projection of the result as a migration gel. The PCR products of mutated founders were sequenced to identify codon-shift mutations.

Abs and flow cytometry

Cellular phenotype was analyzed using the following mAbs from BD Pharmingen: against granulocytes (His48), CD44 (Ox49), TCRαβ (R73), CD45R (His24), CD25 (Ox39), CD4 (Ox35), CD45 (Ox1), and MHC-II (Ox6). Abs used against Foxp3 (FJK-16s; eBioscience), EpCAM (clone GZ.1; Abgent), and anti-AIRE A488 (5H12; eBioscience) and Abs against CD11b/c (Ox42), CD161 (3.2.3), CD45RA (Ox33), TCRγδ (V65), IgM, CD103 (Ox62), CD45RC (Ox22), IgD, 85C7, and CD8 (Ox8) were produced in our laboratory. Abs were used to stain cells, and fluorescence was measured with a BD FACSCanto II flow cytometer (BD Biosciences, Mountain View, CA), and FlowJo software was used to analyze data. Cells were first gated on their morphology, and then dead cells were excluded by staining with fixable viability dye, eFluor 506 (eBioscience).

Cell isolation

Spleen, liver, thymus, and lymph nodes were digested by collagenase D for 30 min at 37°C; the reaction was stopped by adding 0.01 mM EDTA. Cells from blood and bone marrow were also isolated, and RBCs were lysed using a lysis solution (8.29 g NH_4Cl, 1 g $KHCO_3$, 37.2 mg EDTA/1 l deionized water [pH 7.2–7.4]).

Cell sorting

Mesenteric lymph nodes (MLNs) were shredded using 26-gauge needles to extract cells; cells were sorted >99% purity by BD FACSAria (BD Biosciences) by gating on DAPI^{-}TCR^{-}CD103^{+}CD4^{-} (cDC CD4^{-}), CD4^{int} (cDC CD4^{int}), CD4^{+} (cDC CD4^{+}), DAPI^{-}CD45RA^{+} (B cells), DAPI^{-}TCR^{+} (T cells), DAPI^{-}TCR^{-} (non-T cells), and DAPI^{-}EpCAM^{+}Sirpα^{+}CD103^{-}.

In vivo keyhole limpet hemocyanin immunization and in vitro secondary challenge

Aire$^{+/+}$ or *Aire*$^{-/-}$ rats were immunized with keyhole limpet hemocyanin (KLH) protein (Sigma-Aldrich) (100 μg) emulsified (v/v) in 100 μl of CFA (Difco, Lawrence, KS) at the base of the tail. Eleven days after immunization, iliac lymph node cells were extracted and sorted, as described above, in T cells and non-T cells.

T cells were CFSE-labeled (5 nM) (Thermo Fisher Scientific, Waltham, MA) and 50,000 cells were cocultured for 3 d in presence of an equivalent number of non-T cells with or without KLH or OVA (SIINFEKL) at 25 mg/ml in 100 μl of complete RPMI 1640 medium. After 3 d, T cells were stained with anti-TCR Ab, and CFSE dilution was analyzed on BD FACSCanto.

Western blot

Eye, liver, skin, duodenum, salivary gland, ovary, ileum, spleen, kidney, stomach, colon, pancreas, lung, and thymus from *Rag*$^{-/-}$ rat were homogenized in radioimmunoprecipitation lysis buffer. Ten micrograms of protein were run for each organ on a 10% Tris–SDS acrylamide gel and then transferred to a Protran Premium 0.45 NC (0.45 μm) Western membrane (Amersham). The membrane was blocked for 2 h in a TBST solution with 5% milk. The membrane was then incubated with sera from wild type (WT) or *Aire*$^{-/-}$ rat diluted 1/500 overnight at 4°C on constant agitation. After washing the membrane three times in TBST, it was incubated with the secondary Ab HRP-conjugated goat anti-rat IgG (heavy and light) (Jackson Immunoresearch) for 2 h at room temperature on constant agitation. SuperSignal West Pico Chemiluminescent Substrate (Thermo Fisher Scientific) was used as a substrate; photographs were taken by a Fujifilm Las 4000 device.

Transcriptional analysis

mRNA extraction from tissues or cells was performed using an RNeasy Mini Kit (QIAGEN) according to the manufacturer's instruction. After quantification of mRNA, reverse transcription was performed using the Omniscript RT Kit (QIAGEN).

Aire expression level was determined by relative quantitative RT-PCR using TaqMan probes for *Aire* (Rn01428600; Thermo Fisher Scientific) and reported to HPRT expression level (Rn01527840) and TaqMan universal

Master Mix with AmpliTaq Gold (Applied Biosystems). Reaction was performed in StepOnePlus Real-Time PCR Systems.

Total RNA was isolated from thymus using RNeasy Mini Kit (QIAGEN) and was then processed for RNA sequencing. Protocol of 3′ digital gene expression (DGE) RNA sequencing was performed as previously described (19). The differential expression *p* values were processed with DESeq2 (20). Genes were considered as differentially expressed if the Benjamini–Hochberg adjusted *p* value was <0.05. Data were deposited in the European Nucleotides Archive under accession number ERP107351 (https://www.ebi.ac.uk/ena). Genes with altered expression in mice models have been obtained from M. Giraud from the RNA sequencing dataset analysis deposited in the Gene Expression Omnibus under number GSE68190 and GSE87133 (https://www.ncbi.nlm.nih.gov/geo/) (21–23).

Immunofluorescence

Frozen sections of several organs from WT or *Aire*$^{-/-}$ rats were stained with anti–AIRE-A488 (clone 5H12; eBioscience), anti–MHC class II (MHC-II)–Texas Red (BioAtlantic) and anti–EpCAM-purified (clone GZ.1; Abgent). Also, frozen sections of *IgM*$^{-/-}$ rat were used for staining with sera from *Aire*$^{+/+}$ or *Aire*$^{-/-}$ rats. Autoantibodies were revealed using AF488 goat anti-rat IgG (heavy and light) (Invitrogen). After staining, sections were mounted with Prolong Gold Antifade Reagent with DAPI (Molecular Probes) before analysis with confocal microscopy or automated tissue slide scanner (Hamamatsu NanoZoomer Digital Pathology system).

Pathology of autoimmune infiltrations

Eye, liver, skin, duodenum, salivary gland, ovary, testis, ileum, kidney, stomach, colon, pancreas, lung, adrenal gland, axillary lymph node (ALN), and thyroids were fixed in 4% formaldehyde before being embedded in paraffin. Hematoxylin eosin saffron (HES) staining was performed on sections of each organ; the autoimmune score was determined by an anatomopathologist in a blinded manner (A.M.).

Detection of anti-cytokine and anti-dsDNA autoantibodies

Cytokines (IL-22, IL-17F, or IFN-ω; R&D Systems) or salmon sperm DNA (Invitrogen) were coated in a 96-well flat-bottom plate (Thermo Fisher Scientific) in a carbonate buffer overnight at 4°C. After several wash steps, saturation with PBS Tween 20 0.1% BSA 1% was performed for 2 h at 37°C. Sera from WT or *Aire*$^{-/-}$ rats were used as primary Abs (2 h, 37°C), and an HRP-conjugated goat anti-rat IgG (heavy and light) (Jackson Immunoresearch) was used as secondary Ab (2 h, 37°C).

ELISA

For Igs, plates were coated with isotype-specific mouse mAb anti-rat to IgM (MARM-4), IgG (MARG), IgE (MARE), or IgA (MARA) (all from AbD Serotec, Jackson ImmunoResearch, or BD Biosciences) and goat anti-rat IgG1, IgG2a, IgG2b, or IgG2c (Bethyl Laboratories) at 5 μg/ml in PBS overnight at 4°C. After several wash steps, saturation with PBS Tween 0.1% BSA 1% was performed for 2 h at 37°C. Both mouse anti-rat κ and anti-λ chain-specific peroxidase-conjugated Abs (clone MARK-1/MARL-15; AbD Serotec) were added to reveal the staining.

For anti-KLH Abs, plates were coated with KLH at 10 μg/ml in 50 μl of PBS overnight at 4°C. After several wash steps, saturation with PBS Tween 0.1% BSA 1% was performed for 2 h at 37°C. Sera from WT or *Aire*$^{-/-}$ rats were then incubated 2 h at 37°C and washed, and an HRP-conjugated goat anti-rat IgG Ab (heavy and light) (Jackson Immunoresearch) was used (2 h, 37°C) to detect anti-KLH Abs.

Concentration of cytokines in the sera was assessed using a multiplex kit (MILLIPLEX MAP Rat) as recommended by the manufacturer (Merck).

Luciferase immunoprecipitation system assay

Luciferase immunoprecipitation system (LIPS) assays were conducted in 96-well–format plates as described earlier (24). The coding sequences of mouse IFN-α1, IFN-α2, IFN-α4, IFN-α5, IFN-α6, IFN-α7, IFN-α9, IFN-α11, IFN-α13, IFN-α14, and IFN-α16 were cloned into a modified pPK-CMV-F4 fusion vector (PromoCell, Heidelberg, Germany) downstream of the IL-2 signal peptide and the NanoLuc gene from pNL1.3CMV vector (Promega) that was cloned into the plasmid instead of Firefly luciferase. HEK 293 cells were transfected with cloned constructs, and secreted Nanoluc-Ag fusion proteins were collected with the tissue culture supernatant 48 h later. Rat serum dilutions (1:10 or 1:25) were incubated overnight at +4°C with supernatants containing Nanoluc-Ag fusion protein, 10^6 luminescence units per precipitation reaction, either in pools of different IFN-α subtypes, or individually. LIPS assay was performed in 96-well MultiScreen filter HTS plates (Millipore) at room temperature using buffer A (50 mM Tris [pH 7.5], 100 mM NaCl, 5 mM MgCl2, 1% Triton X-100) for all dilutions. Immune complexes from overnight-incubated samples were captured onto Protein G Agarose beads (25 μl of 4% suspension; Exalpha Biologicals). After 1 h, the plate was washed, substrate (fumarazine; Promega) was added, and luminescence intensity was recorded during 5 s with VICTOR ×5 plate reader (PerkinElmer).

Statistical analysis

We used a one- or two-tailed Mann–Whitney *U* test in quantitative PCR, FACS, Western blot, ELISA, LIPS, and luminex experiments.

Results

AIRE is expressed by CD45$^-$MHC-II$^+$ mTECs in the thymus and CD4^{int} cDCs in MLNs in WT rats

We first assessed AIRE expression by flow cytometry in the thymus and quantitative RT-PCR in various organs and tissues, as well as by immunofluorescence and confocal microscopy in the thymus and MLNs. For detection of the AIRE protein, we used a cross-reactive anti-mouse AIRE mAb. In the thymus, AIRE was expressed by flow cytometry in a small subset of CD45$^-$MHC-II$^+$ cells (Fig. 1A). This is in line with intermediate/mature mTEC-specific expression of AIRE. We also observed some AIRE$^+$ cells in the CD45$^-$MHC-II$^-$ cells (Fig. 1A), possibly corresponding to terminally differentiated mTECs (25). Quantitative RT-PCR analysis in lymphoid and nonlymphoid tissues demonstrated a high *Aire* mRNA expression in the thymus and lower levels of expression in spleen, ALNs and MLNs, cecum, colon, testis, and ovary (Fig. 1B). In MLNs, the decreased *Aire* mRNA expression after the dendritic cell (DC) depletion supported the hypothesis that AIRE is expressed preferentially by DCs in these tissues (Fig. 1C). This was confirmed by measurement of *Aire* mRNA level in cell subsets sorted from the MLNs. In rat MLNs, cDC subsets can be distinguished according to their differential expression level of CD4 (26, 27). We also sorted B cells, T cells, and epithelial cells (EpCAM$^+$) (Fig. 1D). We observed that *Aire* mRNA was mostly expressed by CD4^{int} cDCs and to a lesser extent by CD4$^-$ and CD4$^+$ cDCs and epithelial cells in MLNs (Fig. 1D). Immunostaining on thymus and MLNs of AIRE protein expression in combination with MHC-II and EpCAM demonstrated a specific nuclear-dot pattern in the mTECs and coexpression with MHC-II$^+$ and EpCAM$^+$ cells, confirming the pattern of expression of AIRE observed at the transcriptional level (Fig. 1E). In addition, we observed that there was less expression of AIRE in the MLNs compared with the thymus, as demonstrated by the number of spots for a single cell and less AIRE$^+$ cells.

Thus, we conclude that, in the rat, AIRE is expressed in mTECs as well as in a subset of lymph node CD4^{int} cDCs.

Induction of ZFN exon 3–targeted double-strand breaks in Aire *gene from rats results in AIRE deficiency and strong visible autoimmune and ectodermal manifestations*

To date, AIRE deficiency has been induced only in mouse strains showing a mild autoimmune phenotype (15). We observed notable similarities in the organization and layout of the *Aire* locus between humans and rats, whereas mouse *Aire* locus overlaps another gene (Fig. 2A). In contrast to mice, the *Aire* promoter is not inserted into another gene in humans and rats. To generate AIRE-deficient BN rats, we used ZFNs targeting exon 3 [emulating a common R139X mutation in Sardinian APECED patients (28)] in the nuclear localization signal (NLS) sequence to cause a dsDNA cut, generating deletions through nonhomologous end joining, as we had already done in the past (29–31). We microinjected 279 zygotes; 93.43% were transferred and 11.1% gave newborn animals, and among them, 13.6% showed mutations. One of them showed a 17-bp deletion in the NLS sequence, causing a premature stop

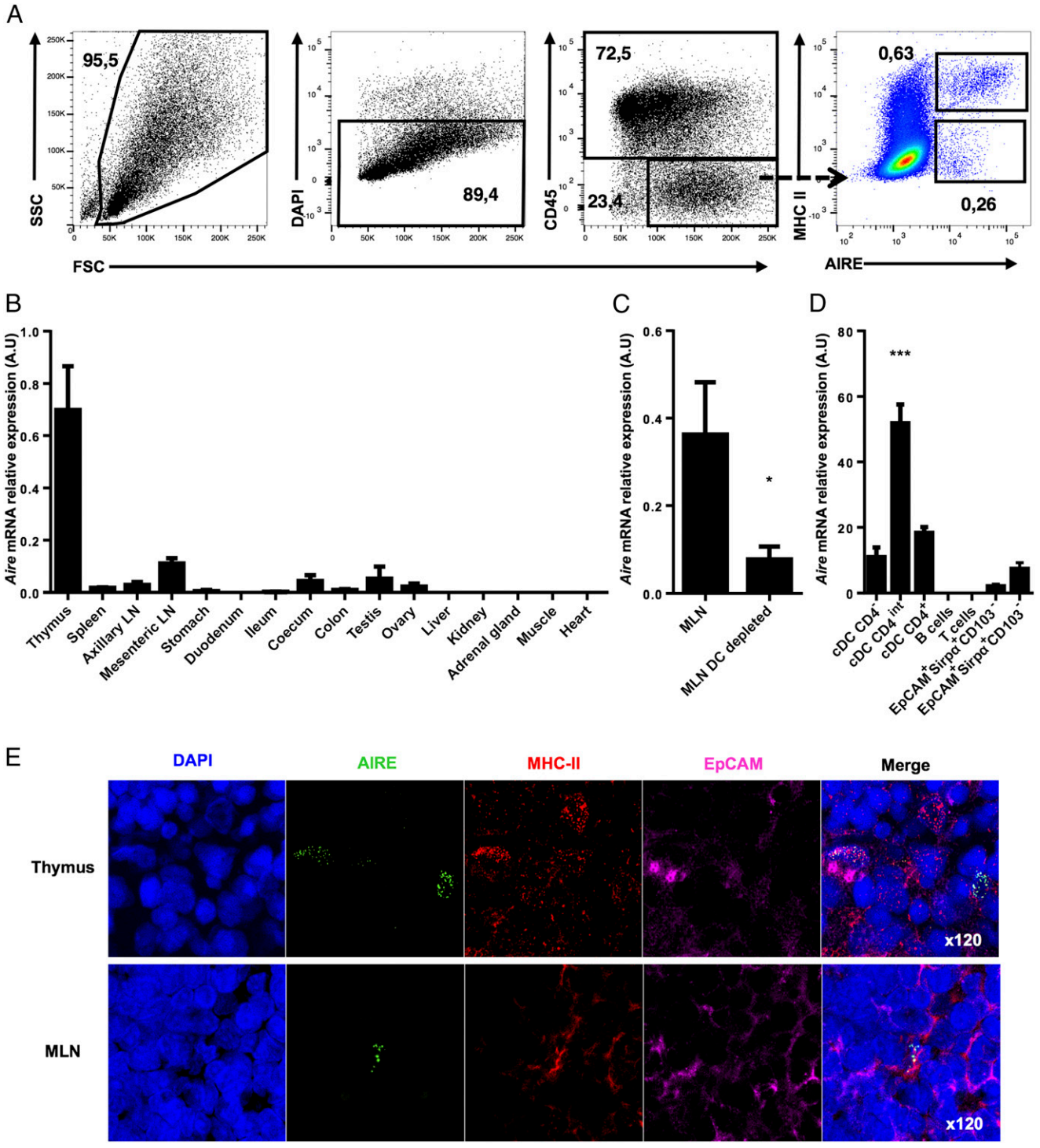

FIGURE 1. AIRE is expressed in the rat at both mRNA and protein level in the thymus and in the periphery. (**A**) mTECs were extracted from the thymus of <3-mo-old male SPD rats and identified as DAPI$^-$, CD45$^-$ and MHC-II and AIRE; expression was analyzed on permeabilized cells by flow cytometry. One representative experiment out of three. (**B**) *Aire* gene relative expression was analyzed by quantitative RT-PCR on total tissues of <6-mo-old male SPD rats. Results are expressed as arbitrary unit (A.U.) of the relative expression of *Aire* reported to *Hprt* expression. ($n = 5$–6). (**C**) *Aire* gene relative expression was analyzed by quantitative RT-PCR on total MLN or DC-depleted MLN by CD103$^-$ negative cell sorting of <6-mo-old male SPD rats ($n = 5$). Results are expressed as A.U. of the relative expression of *Aire* reported to *Hprt* expression. *$p < 0.05$. (**D**) *Aire* gene relative expression was analyzed by RT-quantitative PCR in CD4$^-$, CD4$^+$ and CD4^{int} cDCs, T cells, B cells and epithelial cells in MLN of <6-mo-old male SPD rats ($n = 3$–5). Results are expressed as A.U. of the relative expression of *Aire* reported to *Hprt* expression. ***$p < 0.001$. (**E**) Thymus and MLN sections of <6-mo-old male SPD rats were stained for DAPI (blue), AIRE (green), MHC-II (red) and EpCAM (pink) by immunofluorescence. Results show one representative experiment of four. Merge indicates overlapping DAPI, AIRE, MHC-II, and EpCAM. Original magnification ×120.

codon (Fig. 2B). This founder animal was mated with a WT animal, the mutation was transmitted to the progeny, and homozygous *Aire*$^{-/-}$ were generated. The mutation in the genotype of each mutated rat was confirmed by comparing the WT littermates with heteroduplex mobility assay on an automated microfluidic chip capillary electrophoresis system (32) (Fig. 2C) as well as by sequencing

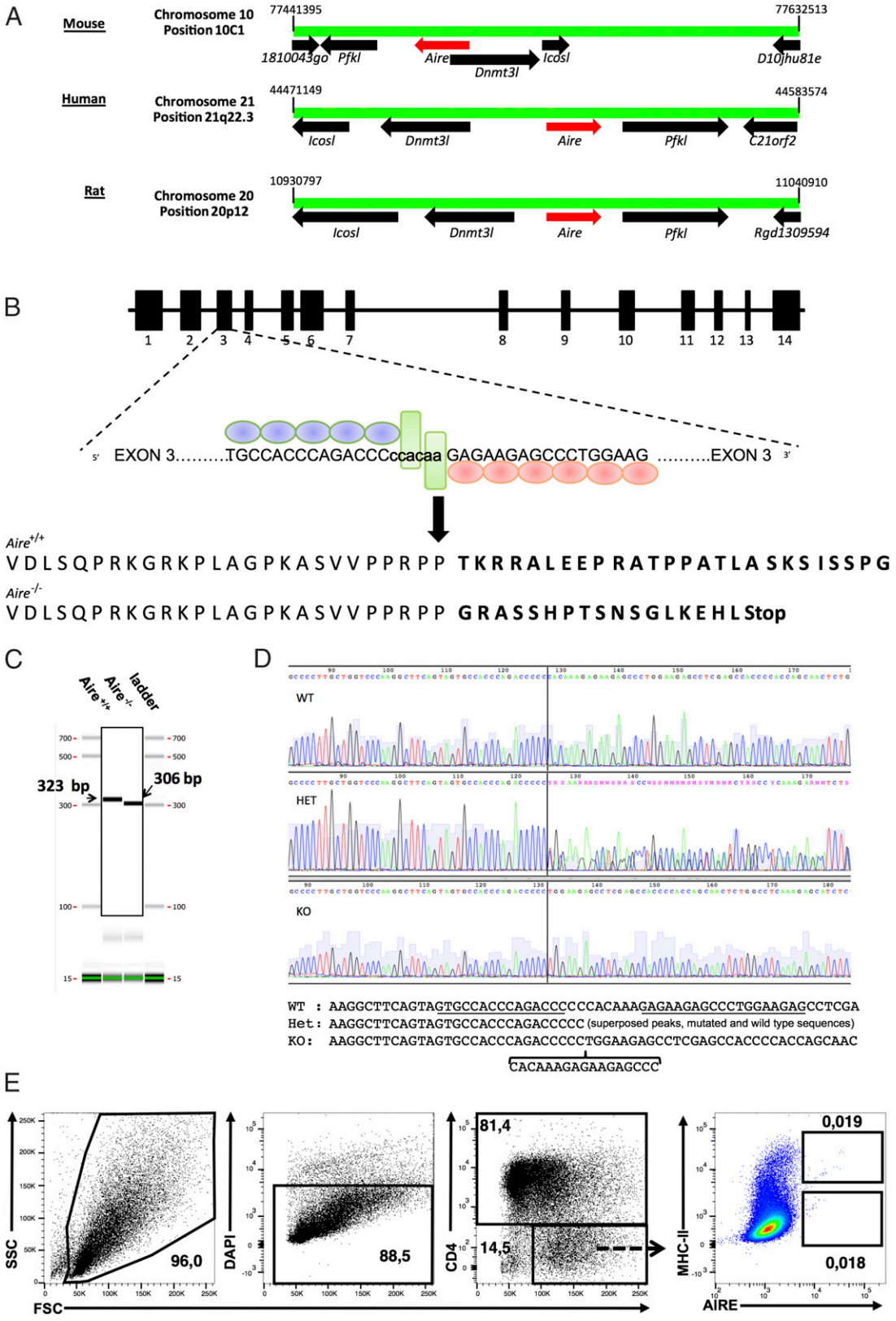

FIGURE 2. Generation of AIRE-deficient rats using ZFNs. (**A**) Illustration of the *Aire* chromosomal gene region (green) in mouse, humans, and rat. Black arrows indicate the position and reading frame of genes. Red arrows indicate the position and reading frame of *Aire* locus. (**B**) Schematic showing that the *Aire* gene was disrupted in the NLS sequence present in exon 3. Black boxes and numbers indicate the different exons. Zinc-finger binding motifs are in blue and red. FokI nuclease is represented in green. (**C**) Genotyping result from tail genomic DNA following automated microfluidic chip capillary electrophoresis system. Scale shown in bp. The two amplicons were obtained with a PCR flanking the target sequence and the one from the $Aire^{-/-}$ animal shows a reduced size versus the WT because of the deletion generated. (**D**) Amplicons were sequenced, and this allowed us to define a deletion of 17 bp in the heterozygous and homozygous animals shown as examples versus a WT rat in the Sanger sequencing chromatograms. Below them, the sequences deduced are shown, and in the WT sequence, the sequences paired with both ZFN arms are underlined. In the homozygous sequence, the deletion of 17 bp is shown. (**E**) AIRE expression was analyzed in mTECs from thymus of $Aire^{-/-}$ of <3-mo-old male SPD rats. mTECs were extracted from the thymus of $Aire^{-/-}$ rats and stained for DAPI and CD45. MHC-II and AIRE expression were analyzed on $DAPI^{-}CD45^{-}$ cells by flow cytometry (representative of four different animals).

(Fig. 2D). The absence of expression of the AIRE protein was further confirmed in the thymus of AIRE-deficient rats (Fig. 2E, compared with Fig. 1A). To determine genetic background dependence of features observed in the $Aire^{-/-}$ BN rats, we backcrossed these animals with the SPD strain for more than six generations.

Breeding of $Aire^{+/-}$ males with $Aire^{+/-}$ females led to a normal gender and genotype litter distribution of the progeny (Table I). We obtained no litter by breeding homozygous $Aire^{-/-}$ males with $Aire^{-/-}$ females in the BN background. The growth and weight of the rats was not affected by AIRE deficiency, at least during the first 20 wk compared with their WT littermates (Fig. 3A).

Altogether, our data show that ZFN efficiently disrupted the *Aire* gene, leading to the absence of the AIRE protein expression.

AIRE deficiency resulted in strong, visible autoimmune and ectodermal manifestations and severe histological abnormalities in the pancreas and skin but slight phenotypic modification of cell subsets

We observed that 100% of AIRE-deficient BN and SPD rats spontaneously developed alopecia and skin depigmentation, observable from the age of 6 mo, compared with their WT littermates (Fig. 3B, 3C, left), as well as nail dystrophy (Fig. 3B, 3C, right), symptoms that correlate with a severe autoimmune disease and that are clinical manifestations regularly found in APECED patients. In addition, the presence of these symptoms was independent of the rat strain genetic background, indicating its correlation with the mutation in the rat *Aire* gene locus.

Measurements of various proteins and enzymes in the blood revealed a slight increase in alkaline phosphatase enzyme and a significant decrease in creatinine levels in $Aire^{-/-}$ rats compared with WT (Fig. 3D), which could suggest kidney dysfunction or liver disease.

To confirm the autoimmune lesions in AIRE-deficient rats, we analyzed various organs and tissues, including thymus, pancreas, skin, liver, lung, salivary gland, testis, ovary, thyroid, spleen, lymph nodes, Peyer patches, stomach, duodenum, ileum, colon, kidney, and eye (Fig. 4). We observed, among the most striking organ lesions, complete macroscopic disappearance of the thymus in 73% of old (>12 mo) $Aire^{-/-}$ rats versus 33% of old $Aire^{+/+}$ rats. In those 27% of $Aire^{-/-}$ rats with detectable thymus, the tissue appeared to have a normal thymic corticomedullary structure (Fig. 4). We also observed severe lesions in the exocrine pancreas, with a decrease in acini and pancreatic fat accumulation, intralobular focal lymphoid infiltration, and hyperplasia of Langerhans islets in 79% of the rats. We further found rare and fragmented hair follicles sometimes associated with minimal peri- and intra-annexial lymphoid infiltrates in the skin in 85% of the rats, a portal lymphoid and plasma cell infiltrate and piecemeal necrosis in the liver in 92% of the rats, and a lymphoid infiltrate in the lung and kidney in 82 and 50% of the rats, respectively. Spleen displayed a follicular hyperplasia in 37.5% of the rats, whereas ovary in 29% of $Aire^{-/-}$ rats displayed an increase in follicles, and testis showed a discrete lymphoid infiltrate. We also found that the ALN displayed

Table I. Gender and litter are not affected by AIRE deficiency

Gender	Genotype	Percentage
Female (49.3%)	$Aire^{+/+}$	20.6
	$Aire^{+/-}$	52.9
	$Aire^{-/-}$	26.5
Male (50.7%)	$Aire^{+/+}$	34.3
	$Aire^{+/-}$	45.7
	$Aire^{-/-}$	20

The percentage of gender and the percentage of litter with $Aire^{+/+}$, $Aire^{+/-}$, and $Aire^{-/-}$ genotypes were analyzed.

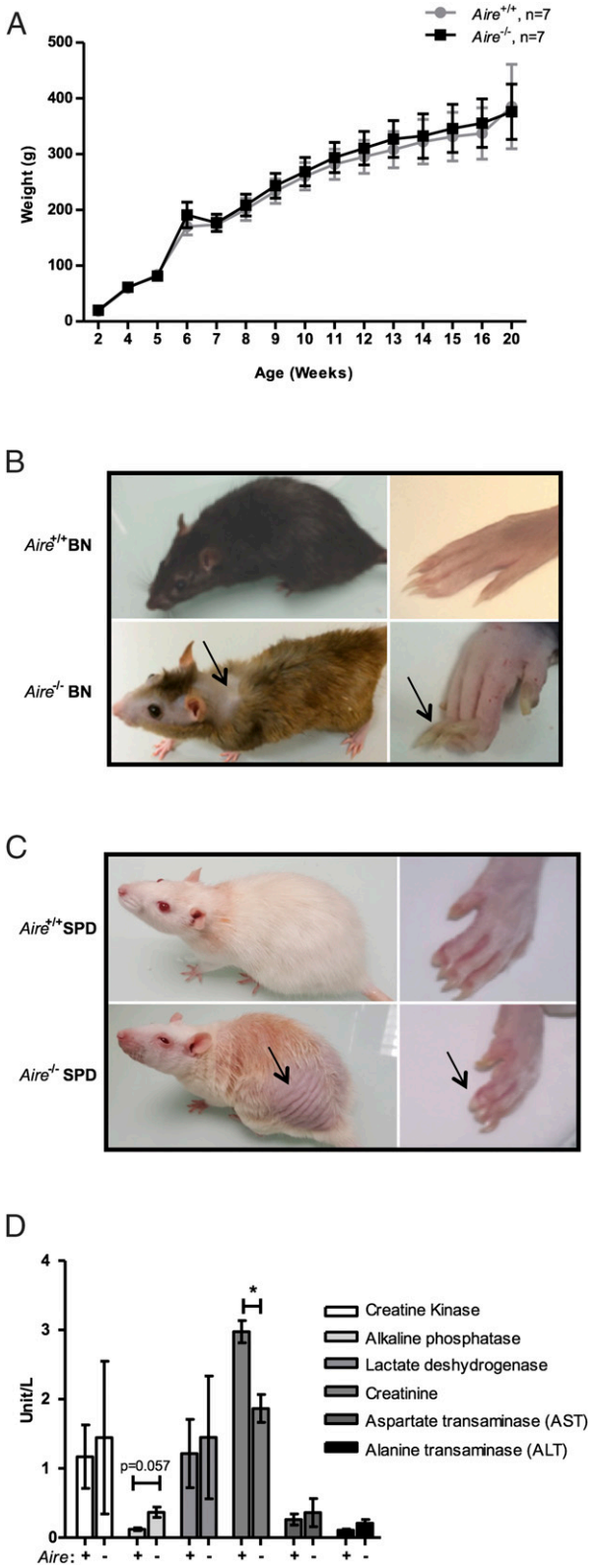

FIGURE 3. $Aire^{-/-}$ rats from BN and SPD strains showed severe autoimmune symptoms. (**A**) Weights of $Aire^{-/-}$ and $Aire^{+/+}$ littermate SPD male and female rats were measured every month during 20 wk following birth. Results are shown as the mean weight ± SEM ($n = 7$). (**B** and **C**) Photographs showing visual aspect of >1-y-old male BN $Aire^{-/-}$ [(B), bottom row] and $Aire^{+/+}$ [(B), top row] littermate rats and male SPD $Aire^{-/-}$ [(C), bottom row] and $Aire^{+/+}$ [(C), top row] littermate rats. General aspect (left) and enlargement on the paw (right). Arrows indicate alopecia, vitiligo, and nail dystrophy. (**D**) Plasma enzymes were quantified in the sera of >1-y-old male and female BN rats. Results are shown as unit per liter for each enzyme ($n = 3$–4.) *$p < 0.05$.

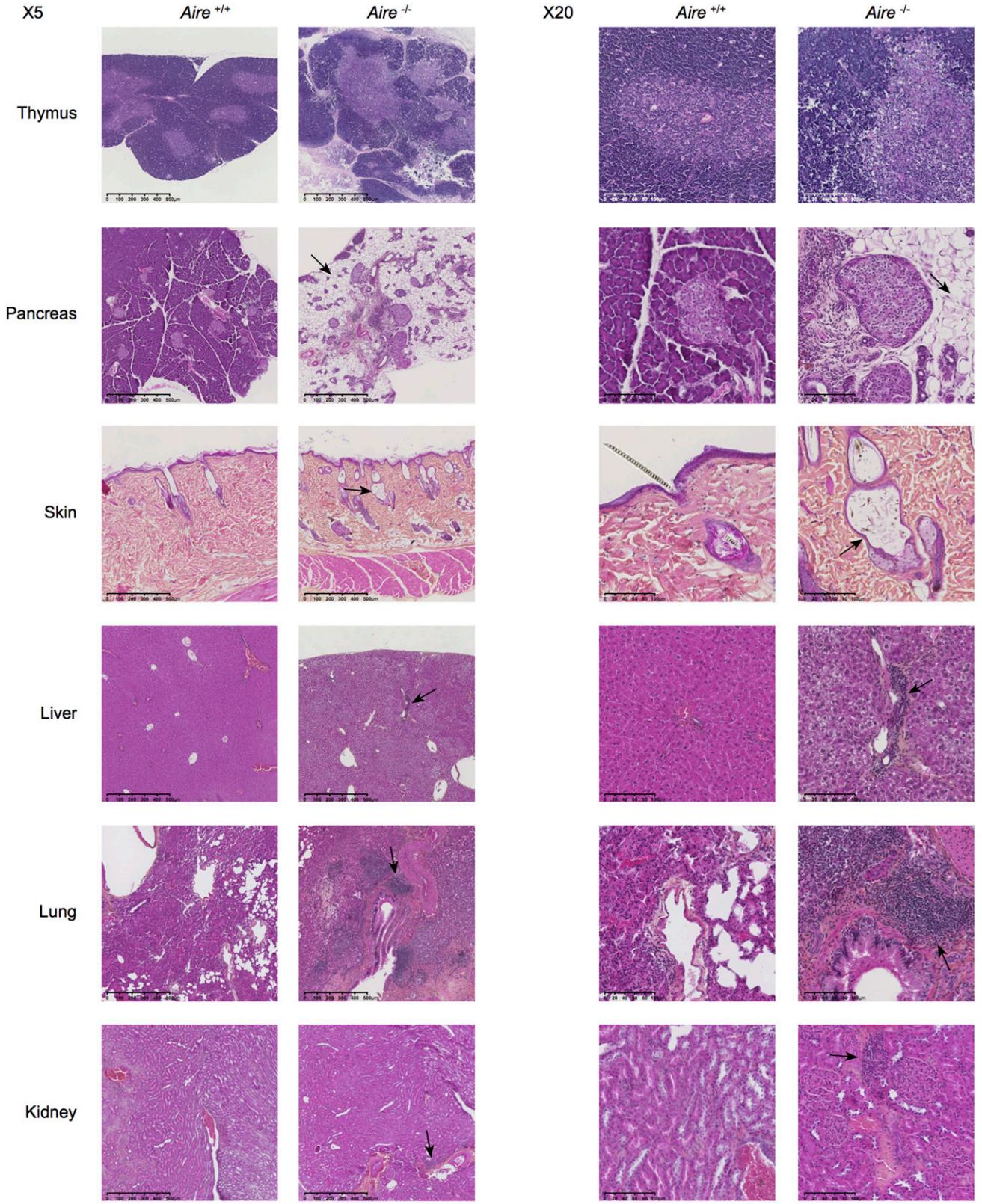

FIGURE 4. $Aire^{-/-}$ rats exhibit severe autoimmune lesions. Thymus, pancreas, skin, liver, lung, and kidney sections of $Aire^{+/+}$ and $Aire^{-/-}$ >12-mo-old (except for thymus <2-mo-old) male and female BN rats were stained with HES. Representative sections of the histological lesions of $Aire^{-/-}$ rats are shown that compare with their WT littermate counterparts. Left panel, Original magnification ×5; left column, $Aire^{+/+}$; right column, $Aire^{-/-}$; right panel, original magnification ×20; left column, $Aire^{+/+}$; right column, $Aire^{-/-}$ (n = 10–12).

a discrete but global hyperplasia in 64% of the rats. In the stomach, we observed a minimal deep lymphoid infiltrate in 25% of the rats. We observed no significant lesions in the Peyer patches, duodenum, ileum, colon, salivary gland, thyroid or adrenal gland, or eye. Finally, we observed that the number of organs with lesions increased over time, with the highest incidence at >10 mo (data not shown).

Altogether, these data confirmed that *Aire*$^{-/-}$ rats developed some of the histological lesions characteristic of APECED disease in humans.

We performed a flow cytometry analysis in the bone marrow, spleen, liver, blood, ALN, and thymus to determine the percentages (Fig. 5, Supplemental Fig. 1) and numbers (data not shown) of cell subsets in *Aire*$^{-/-}$ and *Aire*$^{+/+}$ rats. We observed a decreased percentage of NK cells in the spleen and NKT cells in the bone marrow and the spleen but an increase of both subsets in the liver (Fig. 5A). The analysis of total T cells revealed an increase of activated CD25^{+} T cells in the liver but no differences in CD44 expression (Fig. 5B). Analysis of T cell subsets revealed no significant change, but we saw a trend for an increased percentage of CD4^{+} T cells in the spleen and ALN and an increase in CD4^{+} CD25^{+} T cells, whereas the percentages of CD4^{+}Foxp3^{+} Tregs in the bone marrow were decreased (Fig. 5C). We also found a decrease of CD8^{+} T cells and CD8^{+}CD45RC^{low} Tregs in the blood, a decrease of CD8^{+}CD45RC^{low} Tregs in the ALN, and an increase of CD8^{+}CD45RC^{low} Tregs in the bone marrow (Fig. 5D). B cells and B cell subsets were diminished in the liver, particularly the IgM^{int}IgD^{-} subset (Fig. 5E). We observed an increase in macrophages in the bone marrow, the blood, and the thymus, and an increase in granulocytes in the blood (Fig. 5F). Finally, we observed an increase in CD4^{+} cDCs in the thymus, an increase in CD4^{-} cDCs in the spleen, and a decrease in plasmacytoid dendritic cells in the spleen (Fig. 5G). Although limited, the data, altogether, indicate an impact of AIRE deficiency on the distribution of rat immune cell subsets, with a particularly strong effect on NK and NKT cells.

Aire$^{-/-}$ *rats display high level of circulating autoantibodies targeting organs and cytokines to levels comparable to APECED disease*

We analyzed the expression of cortical thymic epithelial cell genes, mTEC AIRE-independent genes, and mTEC AIRE-dependent genes in the thymus of *Aire*$^{-/-}$ and *Aire*$^{+/+}$ BN rats by DGE-RNA sequencing analysis (15, 21–23) (Fig. 6). DGE-RNA sequencing transcriptional profiling demonstrated that 2422 genes were downregulated and 2288 genes were upregulated in thymus of *Aire*$^{-/-}$ versus *Aire*$^{+/+}$ rats. Results showed that some genes are strongly downregulated in absence of *Aire*, as has been shown in mice. In particular, *Gal*, *Gip*, *Ltf*, *Mt3*, *Mt4*, *Pyy*, *Reg3b*, *Sst*, and *Tac3* were significantly downregulated in *Aire*$^{-/-}$ rats, with *Reg3b*, a pancreas-associated protein, being the most downregulated with a 8.21-fold reduction. Although not significant, we observed that *Fezf2*, a transcription factor independent of *Aire* in mice, was also downregulated in the thymus of *Aire*$^{-/-}$ rats, suggesting that the repertoire of *Aire*-induced genes in the rat might be different from that of the mice. In contrast, other genes, such as *Camp*, *Enos2*, *Loxl3*, or *Timp1*, were not affected by the Aire deficiency. Most cortical thymic epithelial cell genes were not affected by the *Aire* deficiency, although we found that *Psmb11* was significantly downregulated in *Aire*$^{-/-}$ rats. Altogether, these observations demonstrate that some of the genes analyzed in this study were under the control of AIRE in the rat but that there might be some differences in the repertoire of *Aire*-induced genes in the rat.

We investigated the organ-specific autoantibody responses using >6-mo-old male and female *Aire*$^{-/-}$ and *Aire*$^{+/+}$ BN rat sera in Western blotting and immunostaining with confocal microscopy on protein extracts and cryostat sections, respectively, from the tissues of *Rag1*$^{-/-}$ rats, which express low levels of Ig (33) (Fig. 7, Supplemental Fig. 2). Autoantibodies against multiple organ targets were found in all *Aire*$^{-/-}$ sera compared with *Aire*$^{+/+}$ rat sera, and this reactivity was particularly evident in liver, duodenum, salivary gland, kidney, and lung, where several targets per organ were observed; however, it did not correlate with immune infiltrate in the organs because, for example, multiple bands could be observed against the duodenum, whereas minimal lesions and infiltrate were seen by histology (Fig. 7A). Confocal microscopy analysis of organ-specific Abs presents in the sera of *Aire*$^{-/-}$ rats confirmed that several histological structures, in particular, intestines, kidney, liver, testis, adrenal gland, thyroid, and exocrine pancreas, were targeted by the autoantibodies (Fig. 7B, Supplemental Fig. 2). In the liver, a major target in APECED patients, all the hepatocytes were targeted by the autoantibodies. In the digestive tract (duodenum, colon, and ileum), immunofluorescent labeling was localized in microvilli on the surface of the enterocytes. Renal tubular epithelial cells were significantly marked in the kidney. Langerhans islets did not appear to be affected by autoimmunity; however, the pancreas is not spared because the cytoplasm of acini is targeted by autoantibodies, which correlates with the previous histological observations revealing fatty involutions and a rarefaction of acini until the complete disappearance of the exocrine pancreas. On the testis section, a specific marking of the interstitial support tissue was observed, suggesting that the Leydig cells responsible for the production of testosterone were targeted.

To further determine the impact of AIRE deficiency on Ab production, we measured Ig isotypes in the sera of *Aire*$^{-/-}$ versus *Aire*$^{+/+}$ BN (Fig. 8A) and SPD (Supplemental Fig. 3A) rat strains. We observed an increase in IgG1, IgM, and IgA Ab production, whereas levels of other IgG isotypes remained unchanged in *Aire*$^{-/-}$ versus *Aire*$^{+/+}$ BN or SPD rat strains (Fig. 8A), suggesting an abnormal B cell memory compartment and a defect in Ig class switching. The profiling of anti-cytokine Abs by LIPS (24, 34) in both AIRE-deficient rats revealed a high level of Abs when we studied a pool of multiple IFN-α as Ags and separately to IFN-α4 and IFN-α11 subtypes, as well as increased anti–IL-17a Abs (Fig. 8B) to the levels that were comparable to APECED patients (data not shown). We also found high reactivity to IL-6, Tgm4 (autoantigen in prostate), and Vegp2 (autoantigen in salivary gland) in one *Aire*$^{-/-}$ SPD rat only, but did not find high reactivity to Magea4, Magea10, Mageb2, Mlana, Bpifb1, Tyrp1, Tyr, and Pdilt. We observed a slight, but not significant, increase in anti–IL-22, anti–IL-17F, and anti–IFN-ω Abs measured by ELISA (Supplemental Fig. 3A). We observed no differences in the level of anti-dsDNA Abs (Supplemental Fig. 3B). Interestingly, we observed increased levels of circulating IL-1β, IL-10, and TNF-α cytokines in the sera of *Aire*$^{-/-}$ BN rats compared with WT littermates (Fig. 8C).

Finally, we analyzed the involvement of AIRE in T cell responses to self and T and B cells immune responses to nonself (i.e., exogenous Ags) following immunization, and thus the impact of AIRE in T cell help to B cells (Supplemental Fig. 4). T cells purified from spleen of *Aire*$^{-/-}$ rats demonstrated a more important proliferation at day 4 in presence of WT syngeneic non-T cells, by contrast to T cells from *Aire*$^{+/+}$ rats in the presence of WT syngeneic non-T cells (Supplemental Fig. 4A), demonstrating that T cells are biased toward autoreactivity in AIRE-deficient rats. We also stimulated T cells from the lymph node with OVA and observed that the primary T cell response to OVA in vitro was also increased in *Aire*$^{-/-}$ rats compared with WT littermates (Supplemental Fig. 4B). Then, *Aire*$^{-/-}$ rats were immunized with KLH and CFA, and 11 d later, the sera were analyzed for presence of anti-KLH Abs. Following immunization, *Aire*$^{-/-}$ rats and WT littermates developed anti-KLH B and T cell immune responses in a similar manner (Supplemental Fig. 4C), demonstrating that T cell help to B cells and secondary T cell response is not altered in absence of AIRE.

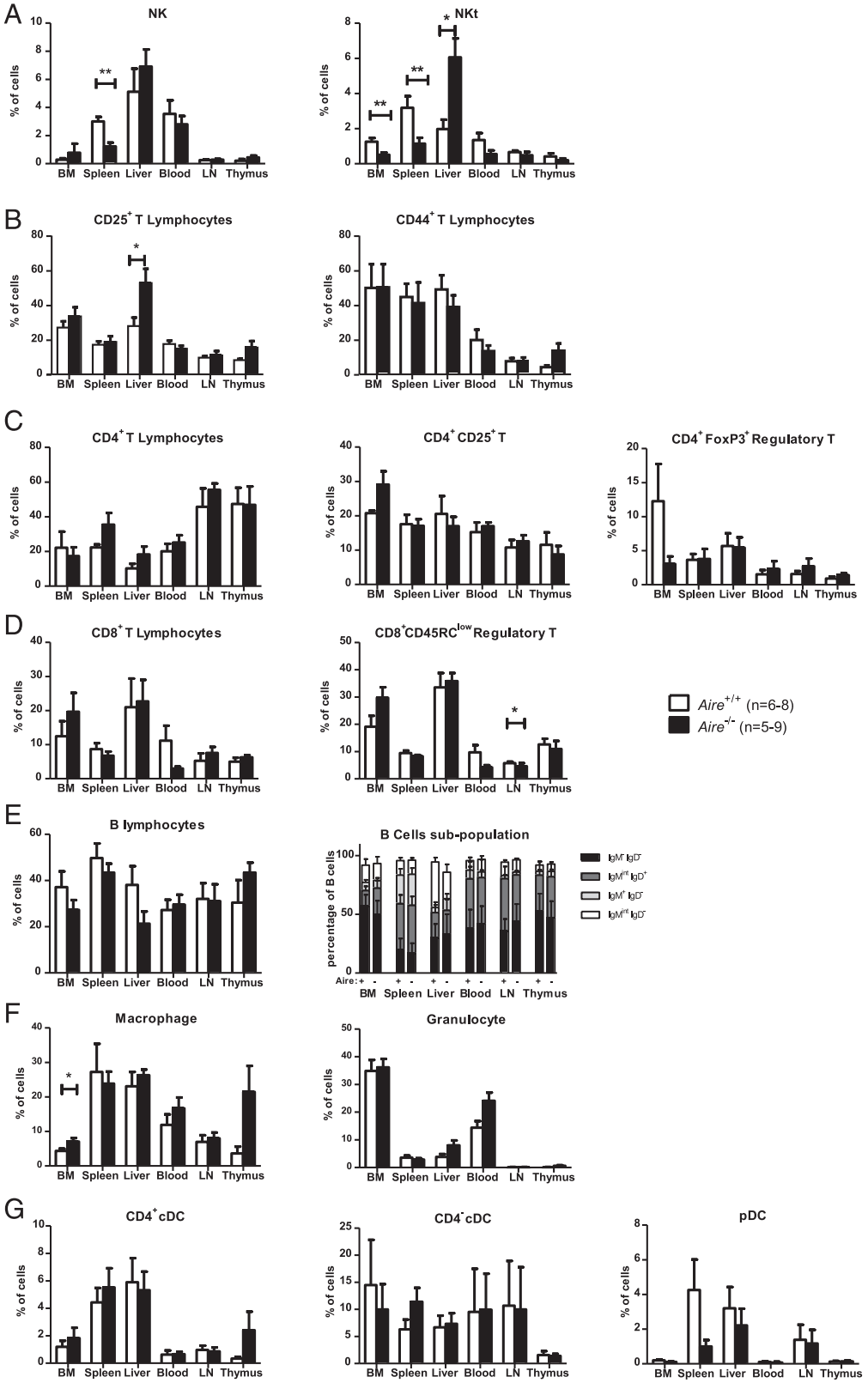

FIGURE 5. Cell subset distribution remained largely unaffected by AIRE deficiency. Percentage of cell subsets was analyzed in bone marrow (BM), spleen, liver, blood, lymph node (LN), and thymus of >12-mo-old male and female BN rats using markers as described in the *Materials and Methods*. (**A**) NK and NKT cells were represented as percentage of living cells for each organ. (**B**) $CD25^+$ and $CD44^+$ T cells were represented as percentage of living TCR^+ cells. (**C**) $CD4^+$ T cells, $CD4^+CD25^+$ T cells, and $CD4^+Foxp3^+$ Tregs were represented as percentage of living TCR^+ cells. (**D**) $CD8^+$ T cells and $CD8^+CD45RC^{low}$ Tregs were represented as percentage of living TCR^+ cells. (**E**) B cells and B cell subpopulations, according to IgM and IgD markers, were represented as a percentage of living cells for each organ. (**F**) Macrophages and granulocytes were represented as a percentage of living cells for each organ. (**G**) $CD4^+$ cDCs, $CD4^-$ cDCs, and plasmacytoid dendritic cells were gated on living TCR^- cells. (A–G) $Aire^{+/+}$ (open bars, n = 6–8) and $Aire^{-/-}$ (filled bars, n = 5–9) percentages are shown as bar graphs representing mean ± SEM; Mann–Whitney U test. $^*p < 0.05$, $^{**}p < 0.01$.

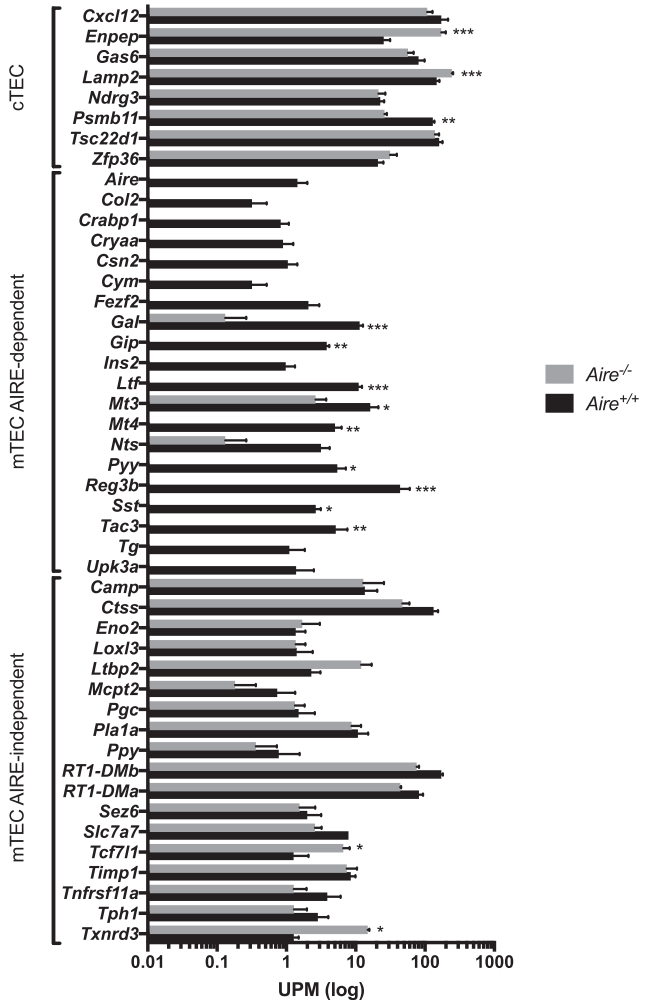

FIGURE 6. Expression of autoantigens in thymus of AIRE-deficient rats. 3′ DGE-RNA sequence analysis was performed on total thymus from $Aire^{+/+}$ ($n = 4$) or $Aire^{-/-}$ ($n = 3$) BN rats. Expression levels of differentially expressed genes are presented according to their unique molecular identifier counts for a gene per million unique molecular identifiers (log scale). $*p < 0.05$, $**p < 0.01$, $***p < 0.001$.

Discussion

Altogether, our data demonstrate that the $Aire^{-/-}$ rat accurately reproduces several characteristics of human APECED disease independently of the genetic background.

In this paper, we describe in rat a natural expression of AIRE in subsets of thymic epithelial cells in the thymus (i.e., a subset in $MHCII^{hi}$ $CD45^{-}$ and a subset in MHC-II^{-} $CD45^{-}$ cells) (Fig. 1). This expression of AIRE in MHC-II^{-} $CD45^{-}$ cells appears to be different from what has been described in the mice models and suggests that mTECs in rat can express AIRE at distinct maturation status [i.e., terminally differentiated mTECs that have lost MHC-II expression but are still expressing AIRE (35, 36) or that are a subset of cells from distinct structures such as Hassall corpuscles, thought to be post-AIRE mTECs that lost their nuclei and merged, which can still express some level of AIRE (25)]. We also observed some expression of AIRE by $CD45^{+}$ cells correlating with expression of AIRE by B cells (data not shown) (37).

In the periphery, we observed that significant levels of *Aire* expression can be detected by quantitative RT-PCR in several organs, but more particularly in the MLN, cecum, and testis and by confocal microscopy in the MLN, demonstrating direct typical dotted nucleic AIRE protein expression. However, in the MLN, very few $AIRE^{+}$ cells could be found by confocal microscopy, compared with the thymus. This expression pattern is in accordance with human AIRE expression in the periphery as shown by transcriptomic analysis (38) and recently published data using immunohistochemical staining and quantitative RT-PCR, suggesting that peripheral AIRE expression supports tissue-specific Ag expression in peripheral lymphoid tissues and negative selection and plays a complementary role to the thymus (39, 40).

Thanks to the ZFN technology (29, 31), we generated a double-strand break in exon 3 of the *Aire* gene, emulating a common mutation in APECED patients (28). Potential for off-target effects was excluded because the rats have been derived for several generations and the symptoms were preserved. In addition, potential off targets edits were all contained within introns and intergenic noncoding regions.

Our data showed that both strains of $Aire^{-/-}$ rats developed histological autoimmune lesions characteristic of APECED, with unique observation of severe alopecia areata observable from 4 to 6 mo of age, a vitiligo-like disease, and nail dystrophy (7) (Fig. 3). The most significant observations made in the mouse model for APECED were observed in the NOD background of the Mathis and Matsumoto mice, with particularly significant damages in liver, pancreas, kidney, and stomach (17, 41). However, they did not observe alopecia, vitiligo, and nail dystrophy, in contrast to human and rat APECED. Thus, $Aire^{-/-}$ rats will be important to provide new insights into the role of AIRE in hair and nail growth and pigmentation of the skin. In human APECED patients, nail and hair lesions have been associated with candidiasis, an infection caused by fungus *Candida albicans* that is likely favored by autoantibodies against Th17-associated cytokines, notably IL-17 and IFN subtypes (7, 42, 43). Although we could not test the susceptibility for candidiasis in our rat model, we observed a strong increase in the levels of neutralizing autoantibodies directed to IL-17 and type 1 IFN subtypes (Fig. 8), suggesting that they could be associated with the lesions in our model. We were able to demonstrate high levels of neutralizing IgG anti-IFN Abs to some subtypes and anti–IL-17α in $Aire^{-/-}$ rat to similar levels observed in APECED patients (44). The presence of several type I IFN autoantibodies in this model is one of the most interesting findings. Meyer et al. (45) recently reported the presence of high-affinity neutralizing autoantibodies to cytokines in APECED patients. Abs with type I IFNs in mouse models of type I diabetes were shown to contribute to the disease (46). However, the role of these Abs in APECED is not clear, and Meyer et al. proposed that naturally arising neutralizing Abs may be beneficial to APECED disease. The presence of anti–type I IFNs could not be evidenced in mouse models of APECED disease; only IgG Abs with IL-17A at older age were found (15, 24), in contrast to the rat model. This finding is surprising and does not fit with the hypothesis that autoantibodies naturally arising in patients with a defect in AIRE, and thus T cell tolerance, may be ameliorating the disease (45), and therapeutic strategies targeting type I IFNs may be assessed in the rat model. Although the dysregulated and impaired T cell–B cell help is one possible origin for those autoantibodies (47), the direct impact of AIRE deficiency on thymic B cell tolerance is also a strong possibility that we cannot exclude and is still an open question that could be assessed in the rat model.

The presence of serum autoantibodies in the AIRE-deficient rats was another indicator of the autoimmune B cell response, although they did not correlate with organ-immune infiltrate (Fig. 7). The liver appeared to be a major target of autoimmunity. In human subjects with APECED, depending on their origins, 3–20% have autoimmune hepatitis, which in the most severe cases is often responsible for death. The enterocytes from the digestive tract were also targeted by autoantibodies. One hypothesis is that the target of these Abs is the glycocalyx, located at the apical pole of these cells. In addition, bronchioles were marked on the lung section, and the

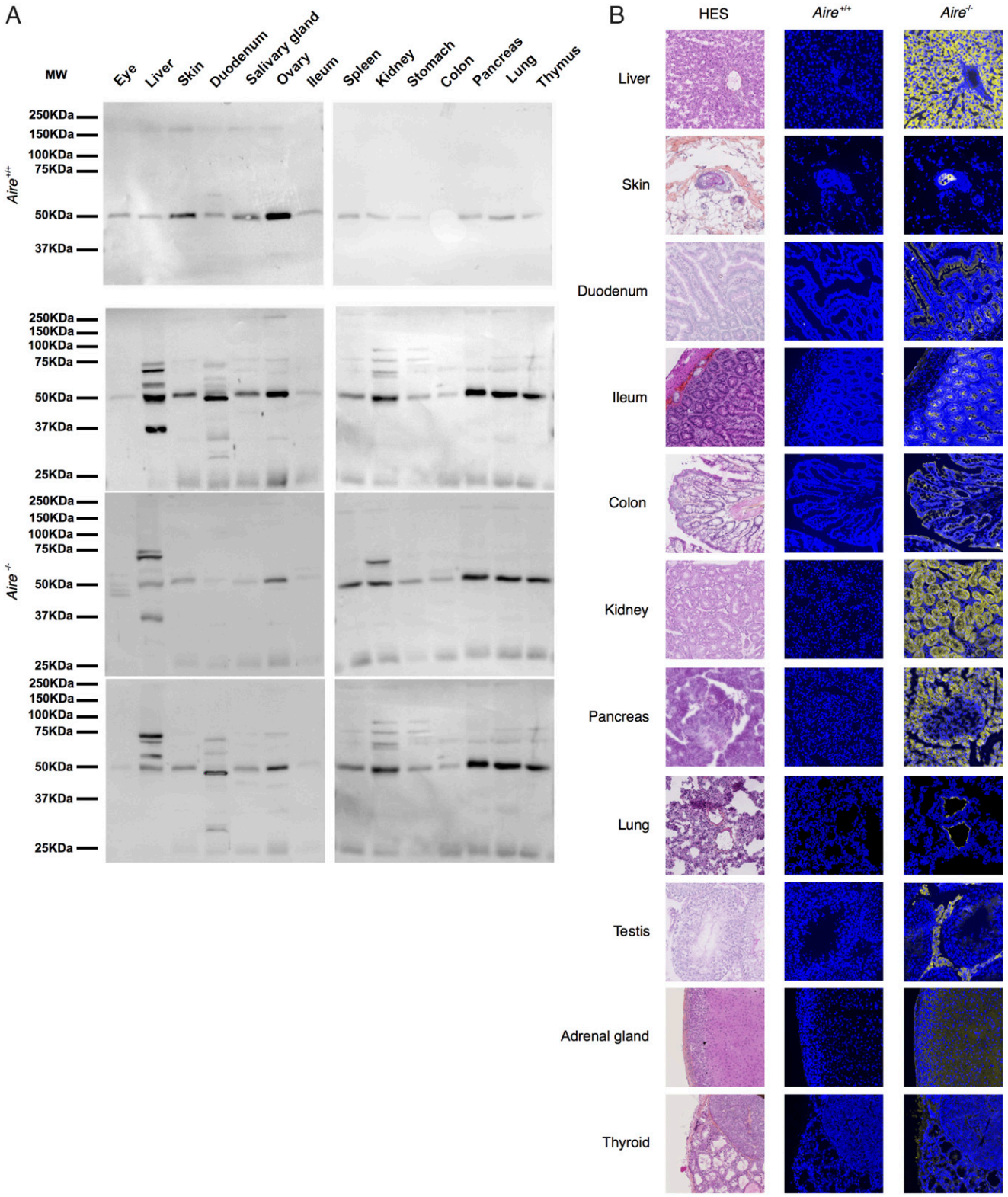

FIGURE 7. *Aire*$^{-/-}$ rats displayed numerous circulating organ-specific autoantibodies. (**A**) Sera from >12-mo-old *Aire*$^{+/+}$ (top row) or *Aire*$^{-/-}$ (three bottom rows) littermate male and female BN rats were incubated on Western blot membranes following migration of individual organs (eye, liver, skin, duodenum, salivary gland, ovary, ileum, spleen, kidney, stomach, colon, pancreas, lung, and thymus) from *Rag*$^{-/-}$ rat. (**B**) Liver, skin, duodenum, ileum, colon, kidney, pancreas, lung, testis, adrenal gland, and thyroid sections of an *IgM*$^{-/-}$ >6-mo-old male rats were stained with HES (left column), DAPI (blue) and *Aire*$^{+/+}$ sera (yellow) (middle column) or DAPI (blue) and *Aire*$^{-/-}$ sera (yellow) (right column) >12-mo-old male and female BN rats (original magnification ×20). Data are representative of four different experiments.

bronchoalveolar epithelial cells also have a glycocalyx on the apical surface. In the testis, the target cells were probably Leydig cells, responsible for the production of testosterone, correlating with the reproductive disorders observed in these animals and also present in patients. Because several bands of the same size were observed in different organs by Western blotting with sera of AIRE-deficient rats

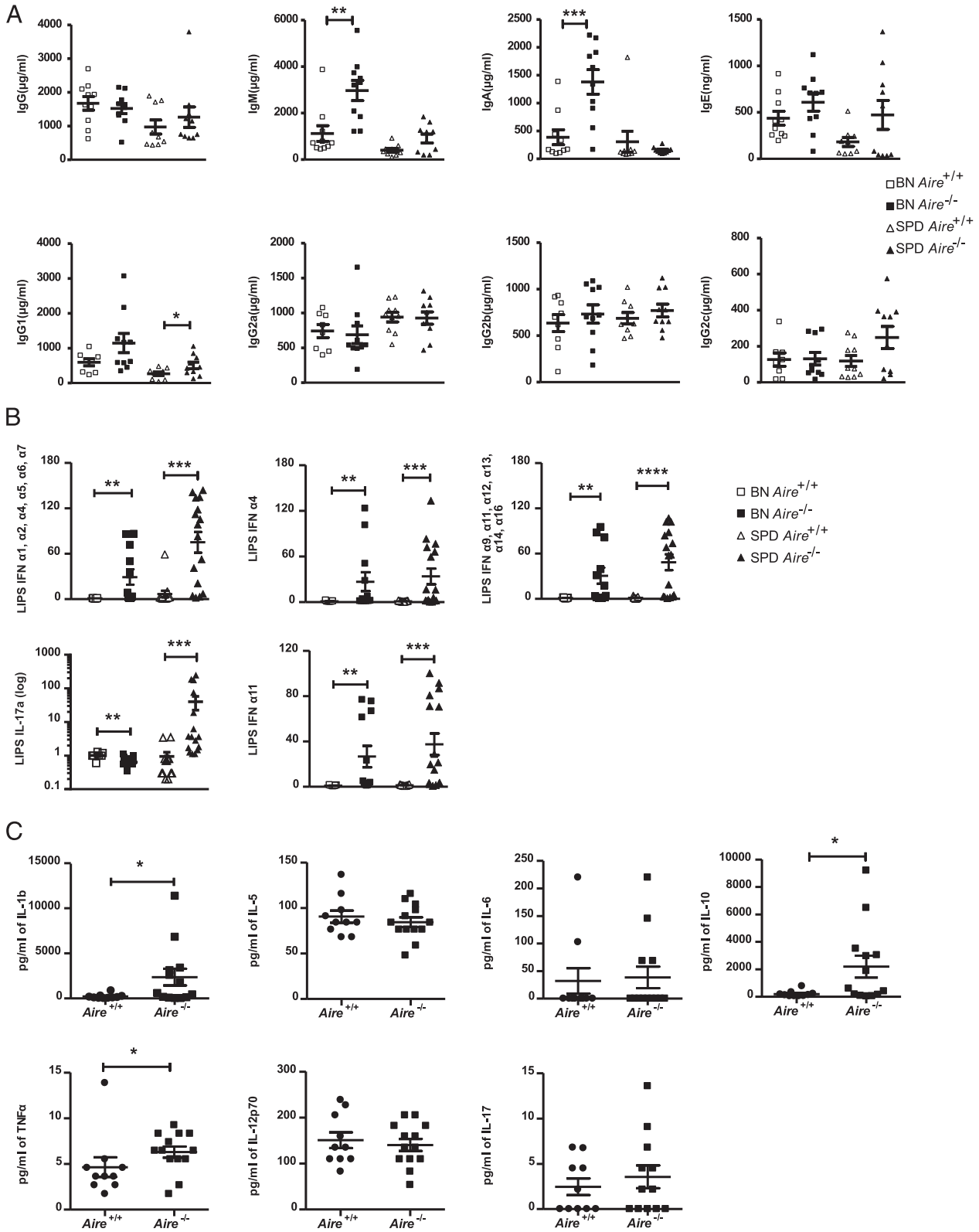

FIGURE 8. Autoimmune symptoms correlate with significant autoantibody production in $Aire^{-/-}$ rats. (**A**) IgG, IgM, IgA, IgE, and IgG subtype 1, 2a, 2b, and 2c concentrations were assessed by ELISA in BN and SPD $Aire^{-/-}$ and $Aire^{+/+}$ sera. Each dot represents the concentration (micrograms per liter) for one animal. Errors bars indicate SEM values (n = 9–10.) One-tailed Mann–Whitney U test, $*p < 0.05$, $**p < 0.01$, $***p < 0.001$. (**B**) Abs to IFN-α1, α2, α4, α5, α6, α7, α9, α11, α12, α13, α14, α16, and IL-17a were tested using LIPS analysis in $Aire^{+/+}$ or $Aire^{-/-}$ sera from BN or SPD rats. Each dot represents a luminescence value (in luminescence units) for one individual; errors bars indicate SEM values (n = 7–16). One-tailed Mann–Whitney U test, $**p < 0.01$, $***p < 0.001$, $****p < 0.0001$. (**C**) Multianalyte profiling was used to detect cytokine concentration in $Aire^{+/+}$ or $Aire^{-/-}$ rat sera. Levels of Il-1β, IL-5, IL-6, IL-17, IL-10, TNF-α, and IL-12p70 were assessed in the sera of BN rat strain. Levels of IL-4 and IFN-γ were not detectable. Results are shown as dot plot graphs representing concentration (picograms per milliliter) ± SEM. One-tailed Mann–Whitney U test, $*p < 0.05$.

(Fig. 7A), it will be interesting to determine in the future, by mass spectrometry, if there are common targets in different organs. We did not find major targets of autoantibodies in the skin, nor did we find a severe infiltration, although we observed that the cells at the base of the hair are stained by autoantibodies (Fig. 7), altogether suggesting that hormones might be targeted by autoantibodies and that APECED is a disease associated with a dysregulation of hormones. Finally, these symptoms were associated with severe organ damages, such as involution of thymic structure, probably due to the dysregulation of the thymopoiesis, and disappearance of exocrine pancreas (Fig. 4). Previous mice models have evidenced the presence of autoantibodies to the pancreas in the sera, but only Matsumoto mice demonstrated exocrine pancreas destruction in 81% of the mice, but preserved β-islets in the NOD background, a background prone to diabetes (41). The BN background is not prone to diabetes, but we still observed major pancreas destruction in 79% of the rats, whereas β cells are preserved, emphasizing the results demonstrated by Matsumoto et al.

In conclusion, the *Aire*$^{-/-}$ rats showed visible, spontaneous autoimmunity along with autoantibody responses, in particular to cytokines, demonstrating that central tolerance mechanisms are altered in *Aire*$^{-/-}$ rats and that this model will be useful and provide new insight into the role of AIRE.

Acknowledgments

We thank Claire Usal, Emmanuel Merieau, and Cécile Braudeau for technical assistance and the MicroPICell platform, Maire Pihlap and Anu Remm for technical help with LIPS assays, and Dimitri Meistermann and Matthieu Giraud for help with the RNA sequencing data. We are most grateful to the Genomics and Bioinformatics Core Facility of Nantes (GenoBiRD, Biogenouest) for technical support and to Crédit Agricole for the donation of the FACSAria.

Disclosures

The authors have no financial conflicts of interest.

References

1. Anderson, M. S., E. S. Venanzi, L. Klein, Z. Chen, S. P. Berzins, S. J. Turley, H. von Boehmer, R. Bronson, A. Dierich, C. Benoist, and D. Mathis. 2002. Projection of an immunological self shadow within the thymus by the aire protein. *Science* 298: 1395–1401.
2. Meredith, M., D. Zemmour, D. Mathis, and C. Benoist. 2015. Aire controls gene expression in the thymic epithelium with ordered stochasticity. *Nat. Immunol.* 16: 942–949.
3. Ahonen, P. 1985. Autoimmune polyendocrinopathy–candidosis–ectodermal dystrophy (APECED): autosomal recessive inheritance. *Clin. Genet.* 27: 535–542.
4. Nagamine, K., P. Peterson, H. S. Scott, J. Kudoh, S. Minoshima, M. Heino, K. J. Krohn, M. D. Lalioti, P. E. Mullis, S. E. Antonarakis, et al. 1997. Positional cloning of the APECED gene. *Nat. Genet.* 17: 393–398.
5. Aaltonen, J., N. Horelli-Kuitunen, J. B. Fan, P. Björses, J. Perheentupa, R. Myers, A. Palotie, and L. Peltonen. 1997. High-resolution physical and transcriptional mapping of the autoimmune polyendocrinopathy-candidiasis-ectodermal dystrophy locus on chromosome 21q22.3 by FISH. *Genome Res.* 7: 820–829.
6. Myhre, A. G., M. Halonen, P. Eskelin, O. Ekwall, H. Hedstrand, F. Rorsman, O. Kämpe, and E. S. Husebye. 2001. Autoimmune polyendocrine syndrome type 1 (APS I) in Norway. *Clin. Endocrinol. (Oxf.)* 54: 211–217.
7. Ahonen, P., S. Myllärniemi, I. Sipilä, and J. Perheentupa. 1990. Clinical variation of autoimmune polyendocrinopathy-candidiasis-ectodermal dystrophy (APECED) in a series of 68 patients. *N. Engl. J. Med.* 322: 1829–1836.
8. Cunnusamy, K., E. J. Baughman, J. Franco, S. B. Ortega, S. Sinha, P. Chaudhary, B. M. Greenberg, E. M. Frohman, and N. J. Karandikar. 2014. Disease exacerbation of multiple sclerosis is characterized by loss of terminally differentiated autoregulatory CD8+ T cells. *Clin. Immunol.* 152: 115–126.
9. Betterle, C., C. Dal Pra, F. Mantero, and R. Zanchetta. 2002. Autoimmune adrenal insufficiency and autoimmune polyendocrine syndromes: autoantibodies, autoantigens, and their applicability in diagnosis and disease prediction. *Endocr. Rev.* 23: 327–364.
10. Husebye, E. S., J. Perheentupa, R. Rautemaa, and O. Kämpe. 2009. Clinical manifestations and management of patients with autoimmune polyendocrine syndrome type I. *J. Intern. Med.* 265: 514–529.
11. Orlova, E. M., A. M. Bukina, E. S. Kuznetsova, M. A. Kareva, E. U. Zakharova, V. A. Peterkova, and I. I. Dedov. 2010. Autoimmune polyglandular syndrome type 1 in Russian patients: clinical variants and autoimmune regulator mutations. *Horm. Res. Paediatr.* 73: 449–457.
12. Alimohammadi, M., P. Björklund, A. Hallgren, N. Pöntynen, G. Szinnai, N. Shikama, M. P. Keller, O. Ekwall, S. A. Kinkel, E. S. Husebye, et al. 2008. Autoimmune polyendocrine syndrome type 1 and NALP5, a parathyroid autoantigen. *N. Engl. J. Med.* 358: 1018–1028.
13. Shum, A. K., M. Alimohammadi, C. L. Tan, M. H. Cheng, T. C. Metzger, C. S. Law, W. Lwin, J. Perheentupa, H. Bour-Jordan, J. C. Carel, et al. 2013. BPIFB1 is a lung-specific autoantigen associated with interstitial lung disease. *Sci. Transl. Med.* 5: 206ra139.
14. Aaltonen, J., P. Björses, J. Perheentupa, N. Horelli-Kuitunen, A. Palotie, L. Peltonen, Y. S. Lee, F. Francis, S. Henning, C. Thiel, et al. 1997. An autoimmune disease, APECED, caused by mutations in a novel gene featuring two PHD-type zinc-finger domains. *Nat. Genet.* 17: 399–403.
15. Hubert, F. X., S. A. Kinkel, P. E. Crewther, P. Z. Cannon, K. E. Webster, M. Link, R. Uibo, M. K. O'Bryan, A. Meager, S. P. Forehan, et al. 2009. Aire-deficient C57BL/6 mice mimicking the common human 13-base pair deletion mutation present with only a mild autoimmune phenotype. *J. Immunol.* 182: 3902–3918.
16. Ramsey, C., O. Winqvist, L. Puhakka, M. Halonen, A. Moro, O. Kämpe, P. Eskelin, M. Pelto-Huikko, and L. Peltonen. 2002. Aire deficient mice develop multiple features of APECED phenotype and show altered immune response. *Hum. Mol. Genet.* 11: 397–409.
17. Smith, T. R., and V. Kumar. 2008. Revival of CD8+ Treg-mediated suppression. *Trends Immunol.* 29: 337–342.
18. Geurts, A. M., G. J. Cost, S. Rémy, X. Cui, L. Tesson, C. Usal, S. Ménoret, H. J. Jacob, I. Anegon, and R. Buelow. 2010. Generation of gene-specific mutated rats using zinc-finger nucleases. *Methods Mol. Biol.* 597: 211–225.
19. Picarda, E., S. Bézie, L. Boucault, E. Autrusseau, S. Kilens, D. Meistermann, B. Martinet, V. Daguin, A. Donnart, E. Charpentier, et al. 2017. Transient antibody targeting of CD45RC induces transplant tolerance and potent antigen-specific regulatory T cells. *JCI Insight* 2: e90088.
20. Love, M. I., W. Huber, and S. Anders. 2014. Moderated estimation of fold change and dispersion for RNA-seq data with DESeq2. *Genome Biol.* 15: 550.
21. Danan-Gotthold, M., C. Guyon, M. Giraud, E. Y. Levanon, and J. Abramson. 2016. Extensive RNA editing and splicing increase immune self-representation diversity in medullary thymic epithelial cells. *Genome Biol.* 17: 219.
22. Chuprin, A., A. Avin, Y. Goldfarb, Y. Herzig, B. Levi, A. Jacob, A. Sela, S. Katz, M. Grossman, C. Guyon, et al. 2015. The deacetylase Sirt1 is an essential regulator of Aire-mediated induction of central immunological tolerance. *Nat. Immunol.* 16: 737–745.
23. Sansom, S. N., N. Shikama-Dorn, S. Zhanybekova, G. Nusspaumer, I. C. Macaulay, M. E. Deadman, A. Heger, C. P. Ponting, and G. A. Holländer. 2014. Population and single-cell genomics reveal the Aire dependency, relief from Polycomb silencing, and distribution of self-antigen expression in thymic epithelia. *Genome Res.* 24: 1918–1931.
24. Kärner, J., A. Meager, M. Laan, J. Maslovskaja, M. Pihlap, A. Remm, E. Juronen, A. S. Wolff, E. S. Husebye, K. T. Podkrajšek, et al. 2013. Anticytokine autoantibodies suggest pathogenetic links with autoimmune regulator deficiency in humans and mice. *Clin. Exp. Immunol.* 171: 263–272.
25. Laan, M., and P. Peterson. 2013. The many faces of aire in central tolerance. *Front. Immunol.* 4: 326.
26. Hubert, F. X., C. Voisine, C. Louvet, M. Heslan, and R. Josien. 2004. Rat plasmacytoid dendritic cells are an abundant subset of MHC class II+ CD4+CD11b-OX62- and type I IFN-producing cells that exhibit selective expression of Toll-like receptors 7 and 9 and strong responsiveness to CpG. *J. Immunol.* 172: 7485–7494.
27. Voisine, C., F. X. Hubert, B. Trinité, M. Heslan, and R. Josien. 2002. Two phenotypically distinct subsets of spleen dendritic cells in rats exhibit different cytokine production and T cell stimulatory activity. *J. Immunol.* 169: 2284–2291.
28. Rosatelli, M. C., A. Meloni, A. Meloni, M. Devoto, A. Cao, H. S. Scott, P. Peterson, M. Heino, K. J. Krohn, K. Nagamine, et al. 1998. A common mutation in Sardinian autoimmune polyendocrinopathy-candidiasis-ectodermal dystrophy patients. *Hum. Genet.* 103: 428–434.
29. Geurts, A. M., G. J. Cost, Y. Freyvert, B. Zeitler, J. C. Miller, V. M. Choi, S. S. Jenkins, A. Wood, X. Cui, X. Meng, et al. 2009. Knockout rats via embryo microinjection of zinc-finger nucleases. *Science* 325: 433.
30. Martin, J. C., G. Bériou, M. Heslan, C. Bossard, A. Jarry, A. Abidi, P. Hulin, S. Ménoret, R. Thinard, I. Anegon, et al. 2016. IL-22BP is produced by eosinophils in human gut and blocks IL-22 protective actions during colitis. *Mucosal Immunol.* 9: 539–549.
31. Rémy, S., L. Tesson, S. Ménoret, C. Usal, A. M. Scharenberg, and I. Anegon. 2010. Zinc-finger nucleases: a powerful tool for genetic engineering of animals. *Transgenic Res.* 19: 363–371.
32. Chenouard, V., L. Brusselle, J. M. Heslan, S. Remy, S. Menoret, C. Usal, L. H. Ouisse, T. H. NGuyen, I. Anegon, and L. Tesson. 2016. A rapid and cost-effective method for genotyping genome-edited animals: a heteroduplex mobility assay using microfluidic capillary electrophoresis. *J. Genet. Genomics.* 43: 341–348.
33. Ménoret, S., S. Fontanière, D. Jantz, L. Tesson, R. Thinard, S. Rémy, C. Usal, L. H. Ouisse, A. Fraichard, and I. Anegon. 2013. Generation of Rag1-knockout immunodeficient rats and mice using engineered meganucleases. *FASEB J.* 27: 703–711.
34. Burbelo, P. D., E. E. Lebovitz, and A. L. Notkins. 2015. Luciferase immunoprecipitation systems for measuring antibodies in autoimmune and infectious diseases. *Transl. Res.* 165: 325–335.
35. Danzl, N. M., S. Jeong, Y. Choi, and K. Alexandropoulos. 2014. Identification of novel thymic epithelial cell subsets whose differentiation is regulated by

RANKL and Traf6. [Published erratum appears in 2014 *PLoS One* 9: e110921.] *PLoS One* 9: e86129.
36. Sun, L., H. Li, H. Luo, and Y. Zhao. 2014. Thymic epithelial cell development and its dysfunction in human diseases. *BioMed Res. Int.* 2014: 206929.
37. Yamano, T., J. Nedjic, M. Hinterberger, M. Steinert, S. Koser, S. Pinto, N. Gerdes, E. Lutgens, N. Ishimaru, M. Busslinger, et al. 2015. Thymic B cells are licensed to present self antigens for central T cell tolerance induction. *Immunity* 42: 1048–1061.
38. Fagerberg, L., B. M. Hallström, P. Oksvold, C. Kampf, D. Djureinovic, J. Odeberg, M. Habuka, S. Tahmasebpoor, A. Danielsson, K. Edlund, et al. 2014. Analysis of the human tissue-specific expression by genome-wide integration of transcriptomics and antibody-based proteomics. *Mol. Cell. Proteomics* 13: 397–406.
39. Peterson, P., T. Org, and A. Rebane. 2008. Transcriptional regulation by AIRE: molecular mechanisms of central tolerance. *Nat. Rev. Immunol.* 8: 948–957.
40. Poliani, P. L., K. Kisand, V. Marrella, M. Ravanini, L. D. Notarangelo, A. Villa, P. Peterson, and F. Facchetti. 2010. Human peripheral lymphoid tissues contain autoimmune regulator-expressing dendritic cells. *Am. J. Pathol.* 176: 1104–1112.
41. Leavy, O. 2010. Regulatory T cells: $CD8^+$ T_{Reg} cells join the fold. *Nat. Rev. Immunol.* 10: 680–681.
42. Meager, A., K. Visvalingam, P. Peterson, K. Möll, A. Murumägi, K. Krohn, P. Eskelin, J. Perheentupa, E. Husebye, Y. Kadota, and N. Willcox. 2006. Anti-interferon autoantibodies in autoimmune polyendocrinopathy syndrome type 1. *PLoS Med.* 3: e289.
43. Kisand, K., A. S. Bøe Wolff, K. T. Podkrajsek, L. Tserel, M. Link, K. V. Kisand, E. Ersvaer, J. Perheentupa, M. M. Erichsen, N. Bratanic, et al. 2010. Chronic mucocutaneous candidiasis in APECED or thymoma patients correlates with autoimmunity to Th17-associated cytokines. *J. Exp. Med.* 207: 299–308.
44. Ito, T., S. Hanabuchi, Y. H. Wang, W. R. Park, K. Arima, L. Bover, F. X. Qin, M. Gilliet, and Y. J. Liu. 2008. Two functional subsets of FOXP3+ regulatory T cells in human thymus and periphery. *Immunity* 28: 870–880.
45. Meyer, S., M. Woodward, C. Hertel, P. Vlaicu, Y. Haque, J. Kärner, A. Macagno, S. C. Onuoha, D. Fishman, H. Peterson, et al; APECED patient collaborative. 2016. AIRE-deficient patients harbor unique high-affinity disease-ameliorating autoantibodies. *Cell* 166: 582–595.
46. Li, Q., B. Xu, S. A. Michie, K. H. Rubins, R. D. Schreriber, and H. O. McDevitt. 2008. Interferon-alpha initiates type 1 diabetes in nonobese diabetic mice. *Proc. Natl. Acad. Sci. USA* 105: 12439–12444.
47. Jung, C. J., S. Ménoret, L. Brusselle, L. Tesson, C. Usal, V. Chenouard, S. Remy, L. H. Ouisse, N. Poirier, B. Vanhove, et al. 2016. Comparative analysis of piggyBac, CRISPR/Cas9 and TALEN mediated BAC transgenesis in the zygote for the generation of humanized SIRPA rats. *Sci. Rep.* 6: 31455.

Fig. Suppl.1

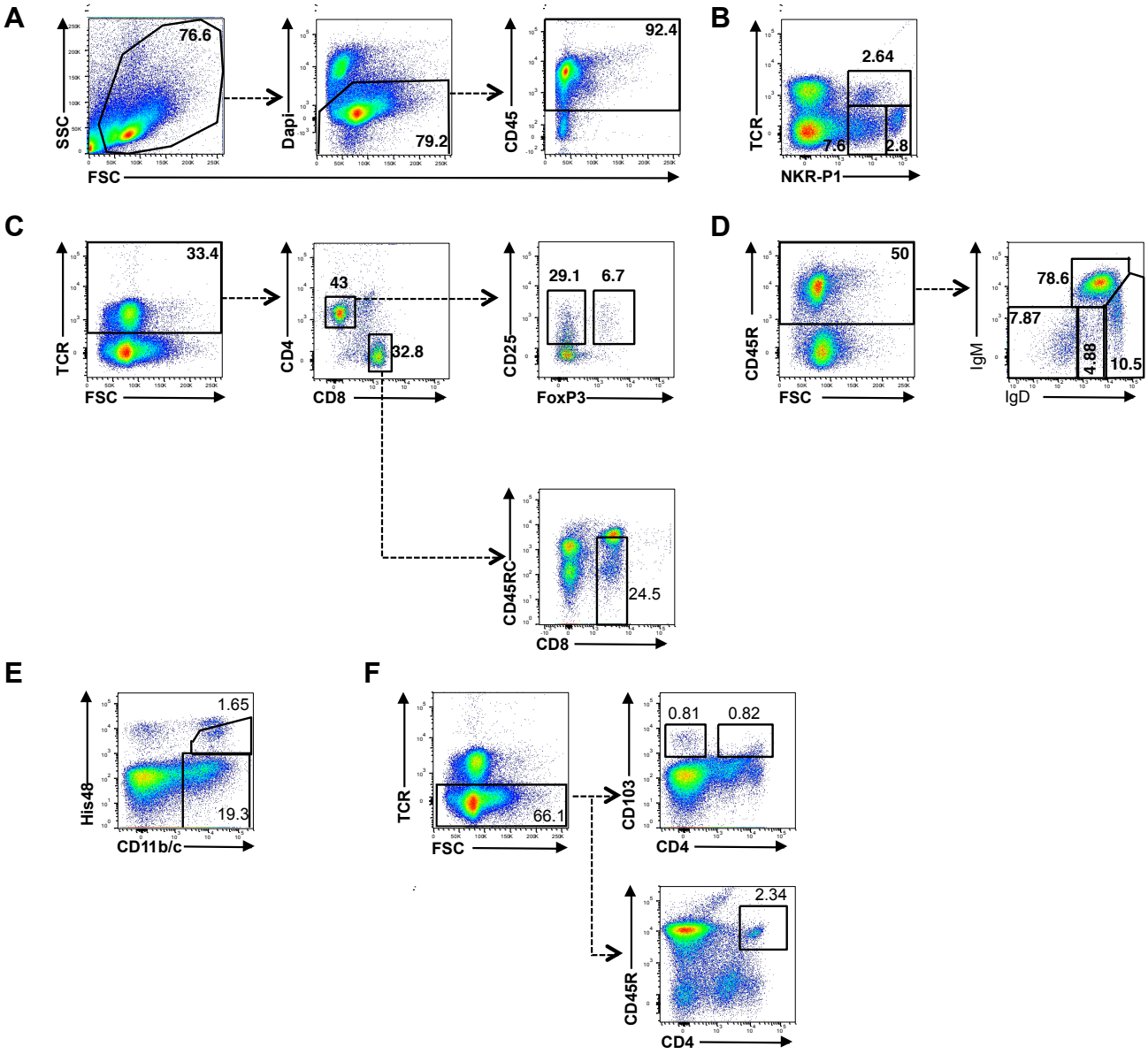

Figure suppl 1. Gating strategy used for FACS analysis showed in figure 5. **A.** General strategy used for the analysis of all subsets gated among living cells CD45$^+$. Gating strategy for **B.** NK cells (TCR$^-$NKR-P1^{hi}) and NKT cells (TCR$^+$NKR-P1$^+$); **C.** CD4$^+$ T lymphocytes (TCR$^+$CD4$^+$), CD4$^+$CD25$^+$ T (TCR$^+$CD4$^+$CD25$^+$), CD4$^+$FoxP3$^+$ regulatory T (TCR$^+$CD4$^+$CD25$^+$FoxP3$^+$), CD8$^+$ lymphocytes (TCR$^+$CD8$^+$) and CD8$^+$CD45RC^{low} regulatory T (TCR$^+$CD8$^+$CD45RC^{low}); **D.** B lymphocytes (CD45RA$^+$) and B cells sub-population (based on IgM and IgD expression); **E.** macrophages (CD11b/c$^+$) and granulocytes (CD11b/c$^+$His48^{int}); **F.** CD4$^+$ cDC (TCR$^-$CD103$^+$CD4$^+$), CD4$^-$ cDC (TCR$^-$CD103$^+$CD4$^-$) and pDC (TCR$^-$CD45R$^+$CD4$^+$).

Fig. Suppl. 2

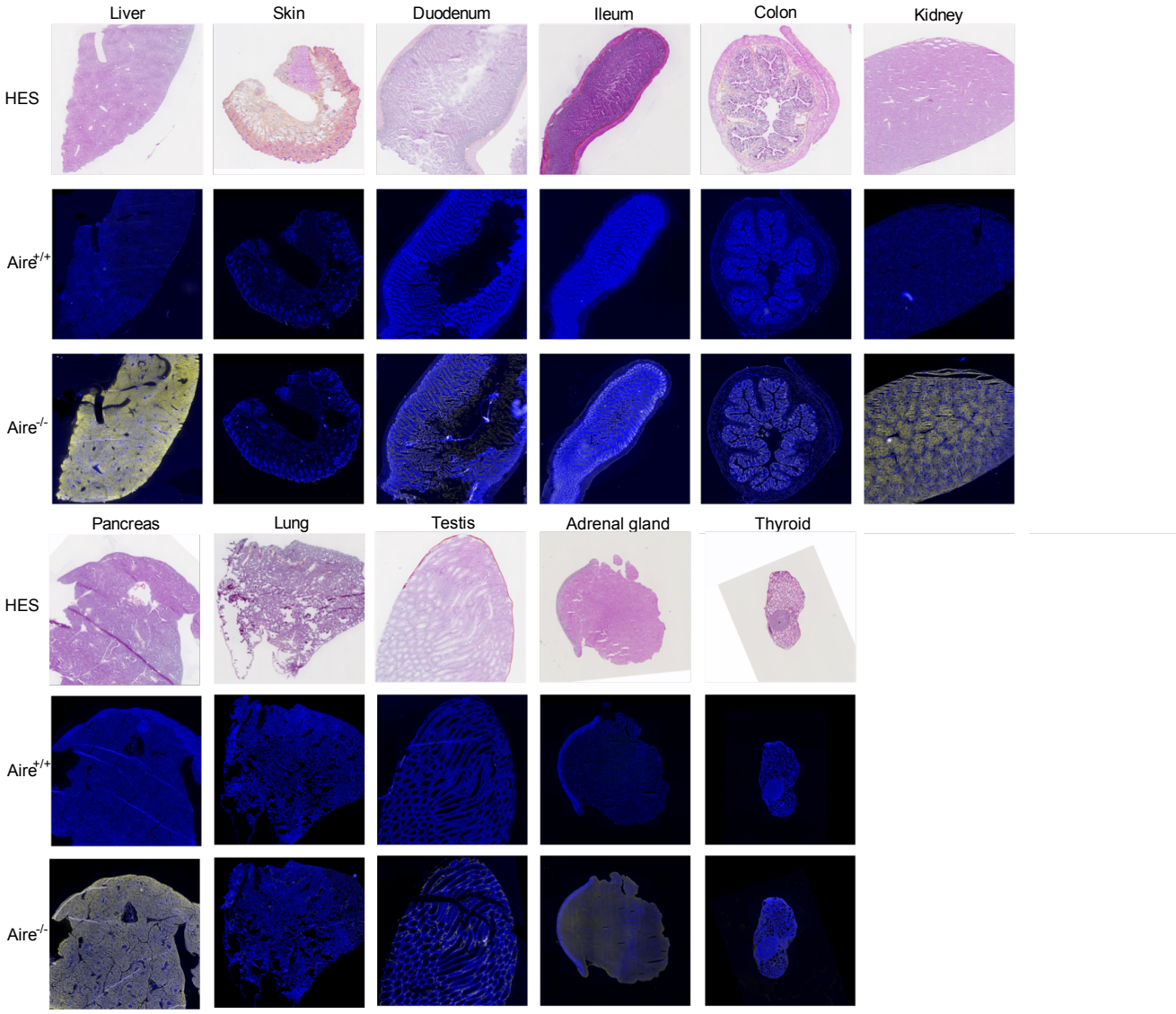

Figure suppl 2. Autoantibodies directed to organs were analyzed in Aire$^{-/-}$ rats. Liver, skin, duodenum, ileum, colon, kidney, pancreas, spleen, MLN, lung, testis, adrenal gland and thyroid sections of *IgM*$^{-/-}$ rats were stained with HES (top row), Dapi (blue) and *Aire*$^{+/+}$ sera (yellow) (middle row) or Dapi (blue) and *Aire*$^{-/-}$sera (yellow) (bottom row) (x2.5). Data are representative of 4 different experiments.

Fig. Suppl. 3

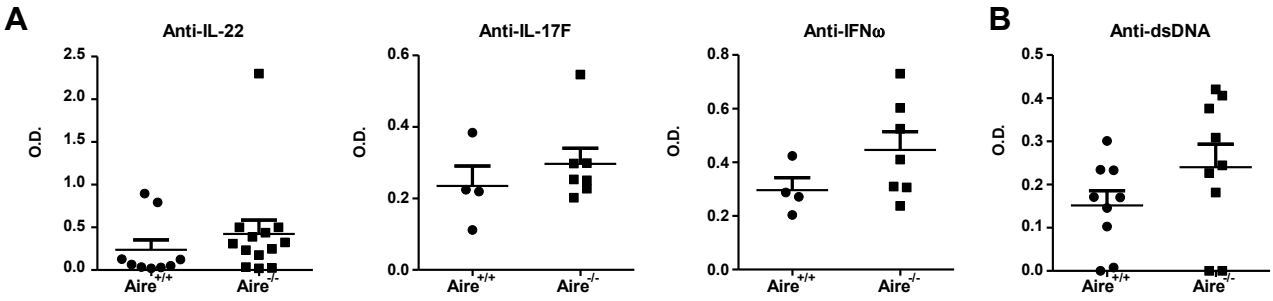

Figure suppl 3. Autoantibodies directed to cytokine were analyzed in Aire$^{-/-}$ rats. The presence of auto-antibodies was analyzed by ELISA after coating of **A.** the cytokines of interest or **B.** salmon sperm DNA and incubation with sera from *Aire*$^{+/+}$ or *Aire*$^{-/-}$ rats. Each dot represents an animal. Results are expressed as mean of optical density (O.D.) +/- SEM.

Fig. Suppl. 4

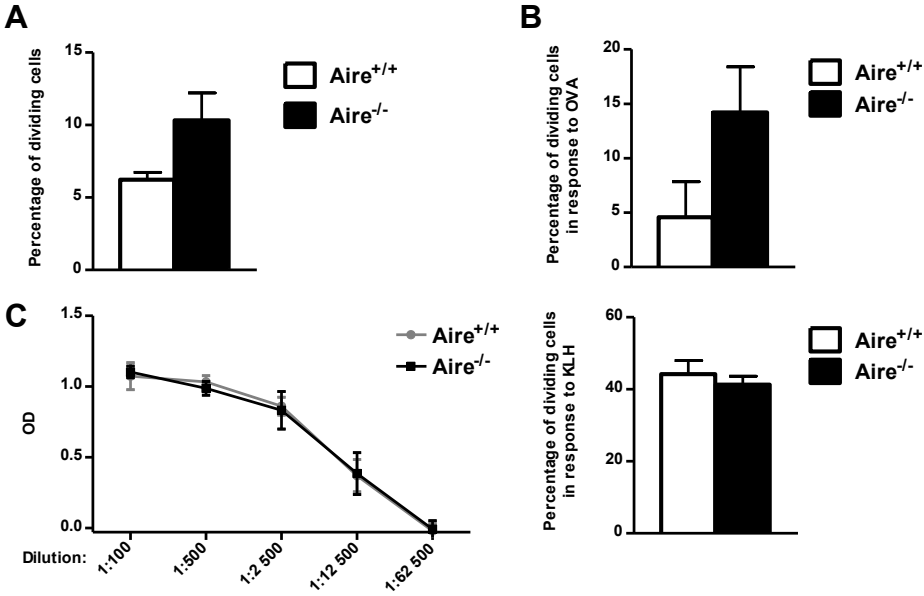

Figure Suppl. 4. A biased primary T cell response to self and non-self, but not secondary response was observed in AIRE-deficient rats. T cells from the draining lymph nodes were collected 11 days after KLH immunization in the footpad. **A.** CFSE-labeled T cells from *Aire*$^{-/-}$ or *Aire*$^{+/+}$ of < 6 months old male SPD rats were incubated for 4 days in presence of non-T cells from *Aire*$^{+/+}$ of < 6 months old male SPD rats and analyzed for their proliferation. Bar graphs show the mean ± SEM percentage of dividing cells (n=3-4). **B.** CFSE-labeled T cells from *Aire*$^{-/-}$ or *Aire*$^{+/+}$ of < 6 months old male SPD rats were incubated for 4 days in presence of non-T cells from *Aire*$^{+/+}$ rats and OVA and analyzed for their proliferation. Background T cells proliferation in absence of OVA was subtracted and results are expressed as mean percentage of dividing cells in response to OVA ± SEM (n=4-6). **C.** Left, Presence of anti-KLH-specific antibodies was assessed by ELISA. Optical density was measured for different sera dilution (x axis) (n=3) in *Aire*$^{-/-}$ or *Aire*$^{+/+}$ of < 6 months old male SPD rats 11 days after immunization. Right, CFSE-labeled T cells from *Aire*$^{-/-}$ or *Aire*$^{+/+}$ of < 6 months old male SPD rats were incubated for 4 days in presence of non-T cells from *Aire*$^{+/+}$ of < 6 months old male SPD rats and KLH and analyzed for their proliferation. Background T cells proliferation in absence of KLH was subtracted and results are expressed as mean percentage of dividing cells in response to KLH ± SEM (n=4-6).